UNIVERSITATEA POLITEHNICA DIN BUCUREŞTI

Facultatea de Ştiinţe Aplicate

Şcoala Doctorală de Ştiinţe Aplicate

PHD THESIS SUMMARY

SYNTHESIS OF PLATINUM NANOPARTICLES BY PULSED LASER ABLATION IN LIQUID MEDIUM METHOD USING THE KrF EXCIMER LASER

Doctorand

Oana – Andreea LAZĂR

Conducător Ştiintific

Prof. Dr.rer.nat. Marius ENĂCHESCU

București, 2023

CONTENT

AIM OF THE WORK AND THESIS PRESENTATION

Nanotechnology, defined as "any technology that allows construction at the nano scale with applications in the real world", has experienced a spectacular evolution, contributing significantly to technological progress in various scientific fields, such as: physics, chemistry, biology, materials science, medicine or pharmacy. Nanostructured materials (for example: metals, alloys, semiconductors, polymers), due to the specific physico-chemical properties they possess, including: size, surface-volume ratio and purity, allow the development of new structures, systems or devices with a potential widely applicable in nano-electronics, health, energy or biotechnology [1].În funcție de metoda de sinteză și parametrii folosiți se pot construi

arhitecturi diferite, cu proprietăţi controlate. Thus, the specificity of nanomaterials is closely related to the method of preparation, because even a slight change in the working conditions can cause a significant change in their characteristics [1,2].

Each nanomaterials preparation procedure is characterized by a series of advantages and disadvantages. Traditional synthesis methods such as: thermal decomposition, chemical reduction, hydrolysis, solvothermal, hydrothermal, electrochemical or physical methods usually require relatively expensive chemical precursors, involve ligand exchange reactions, use stabilizing agents or surfactants and generate a series of secondary products with a certain level of toxicity [3-5]. Consequently, it is expected that progress in the field of synthesis techniques will lead to overcoming the disadvantages mentioned above and improve the functionality and purity of the obtained nanomaterials.

In the last decades, special attention has been paid to the synthesis methods using the pulsed laser, considered as effective techniques both for obtaining a wide range of nanostructured or sub-micron sized materials, as well as for the rigorous control of the surface and the electronic structure and / or their crystals. The interaction of the laser with the source material can take place in different environments, thus facilitating the production of different materials. Synthesis procedures using the pulsed laser, by optimizing the main control parameters including: the wavelength of the pulsed laser, the applied energy, the reaction time, the repetition rate and the nature of the solvent, offer a series of advantages compared to conventional chemical and physical routes, for a much finer control of the dimensions, composition, surface and crystalline structure, later correlated with the catalytic, electronic, thermal, optical and mechanical properties of the produced nanomaterial [4,6,7].

Synthetically, the main advantages of synthesis methodologies using the pulsed laser are [6,7]:

- represents a process belonging to "green chemistry", because it does not require the additional use of complexing agents, reducing agents or surfactants. Under these conditions, the catalytically active areas of the nanoparticles are not blocked by the presence of molecules that adhere to the surface of the atoms;

- the synthesis process does not result in potentially toxic secondary reaction products, so it is considered a method with minimal impact on the environment;

- the experimental setup is relatively simple and a little expensive;

The method of synthesis of nanomaterials using the pulsed laser allows obtaining uniform nanoparticles from a dimensional point of view. Also, gram quantities can be produced for relatively short ablation times, depending on the applied repetition rate, so it is considered suitable for industrial uses. In the field of nanomaterial synthesis, great interest has been given in recent years to the use of the pulsed laser ablation in liquid method (*Pulsed Laser Ablation in Liquids, PLAL*), with the help of which various types of nanomaterials characterized by specific morphologies, phases and structures have been obtained , through a process having only one stage. Moreover, they have proven particularly attractive for applications in the field of sensors, catalysts/electrocatalysts, optical devices, as well as in the biomedical field.

Metallic nanoparticles belonging to the class of zero-dimensional nanomaterials (0-D) are of particular importance due to the unique optical and electrical properties they possess, which facilitates their use in a wide range of applications [1,2].

Among them, Pt nanoparticles are widely used as catalysts in various industrial processes and in the automotive industry, as well as in the fields of energy and environmental protection, especially due to the advantages they offer, in terms of selectivity, lifetime , or of the reuse potential. Belonging to the group of noble metals, platinum is characterized by high stability against oxidation and corrosion processes. Due to its high catalytic activity, Pt is an essential catalyst for the electrochemical reactions that take place in the operation of fuel cells and in the production of hydrogen through the electrolysis of water, improving the yield of the oxidation reactions of hydrogen and oxygen (HOR, ORR), as well as the reaction of hydrogen reduction (HER) [7-9].

In this context, the objective of this work is to study the obtaining and characterization of platinum nanoparticles applying the pulsed laser ablation method using the KrF excimer laser, using different liquid media, respectively: (i) bidistilled water; (ii) aqueous solutions of ethanol with different concentrations; (iii) aqueous solutions of isopropanol having different concentrations; and (iv) systems of "analog ionic liquids" or eutectic solvents (Deep Eutectic Solvents, denoted DES) which are based on eutectic mixtures of choline chloride as hydrogen bond acceptor (HBA) with compounds acting as bond donors of hydrogen (HBD), respectively: urea, glycerin and ethylene glycol. Additionally, the colloidal solutions based on Pt nanoparticles synthesized using pulsed laser ablation in liquid media were subsequently applied to improve the signal during the detection of an organic compound, respectively

methylene blue, by the method of surface-enhanced Raman spectroscopy, SERS (*Surface Enhanced Raman Spectroscopy*).

The doctoral thesis includes six chapters, of which the first presents the literature study, and five present the original contributions.

Chapter 1, the first chapter from the literature section, describes the published results regarding the pulsed laser ablation method in liquid medium, including information regarding the main operating parameters, including: laser wavelength, fluence and repetition rate, target and nature of liquid medium . Next, results from the literature regarding the synthesis of different types of metallic nanoparticles using the PLAL technique are presented, as well as the associated areas of applicability.

The part of original contributions begins with **chapter 2** which presents in detail a series of experimental techniques that were used both for the synthesis by laser ablation in a liquid medium of Pt nanoparticles, as well as for their characterization, capitalizing on the existing high performance infrastructure within the laboratories Center for Surface Science and Nanotechnology (CSSNT) from the Polytechnic University of Bucharest.

Chapters 3, 4, 5 and 6 present the investigations carried out regarding the synthesis of Pt nanoparticles using the PLAL method and different liquid media, respectively: double-distilled water, aqueous solutions of ethanol and isopropanol in different concentrations, as well as eutectic solvent systems based on mixtures eutectics of choline chloride with urea, glycerin and ethylene glycol. The possibility of synthesizing Pt nanoparticles with very small average sizes, of the order of 1 - 4 nm, was demonstrated. The influence of the technological parameters of the ablation method, including the laser fluence, the repetition rate, the ablation time and the liquid medium used, on the morphological and structural characteristics of the obtained Pt nanoparticles is presented in detail. Also, the possibility of applying the Pt nanoparticles thus synthesized for the detection of an organic compound, namely methylene blue, by means of the Raman spectroscopy method with surface amplification, SERS, was also investigated.

The doctoral thesis ends with the final conclusions and the prospects for further development.

At the end of each chapter, the consulted bibliographic references are also included.

The original results from the thesis were capitalized by publishing a number of 18 articles in ISI rated specialized magazines, 2 book chapters, as well as by presentations at 12 international conferences.

CHAPTER 1. GENERAL PRESENTATION OF THE LITERATURE ON THE PULSED LASER ABLATION IN LIQUID METHOD FOR THE SYNTHESIS OF Pt NANOPARTICLES

1.1. INTRODUCTION

The first ruby crystal laser was developed by Maiman nearly 60 years ago in Hughes Research Laboratories and was applied in the irradiation and production of various nanomaterials. [10-12] After its appearance, the pulsed laser ablation (PLA) method) has been used to fabricate different types of nanostructures such as: thin films (TF), nanoparticles (NPs), nanowires (nanowires-NW) or nanoscale networks (NNW) which have been used in various applications[13-16].

In general, nanomaterials, due to the unique properties they possess, can be used in a wide range of applications in various fields, including: catalysis, water treatment, energy storage, medicine or agriculture [17-19]. Two effects determine the significantly different behavior of nanomaterials compared to that of the "bulk" materials from which they are produced, respectively: surface effects and quantum effects [20]. They facilitate the improvement of nanomaterials with new catalytic, mechanical, thermal, magnetic, electronic and optical properties [21-23]. The surface effects occurring in nanomaterials are different compared to those present in micromaterials or in bulk materials because: (a) dispersed nanomaterials have a very large surface area and a large number of particles per unit mass, (b) the fraction of atoms of on the surface in nanomaterials is increased and (c) atoms located on the surface in nanomaterials have fewer direct neighbors [20,23]. Therefore, as a consequence of each of these differences, the physical and chemical properties of nanomaterials change compared to the larger materials of which they are composed. Normally, large surface areas and high surface-to-volume ratios develop the reactivity of nanomaterials due to the larger reaction surface [23] leading to significant effects of surface properties on their structure [18].

Furthermore, the dispersion of nanomaterials is a key element for surface effects. Strong attractive interactions between NPs can lead to the agglomeration and aggregation of nanomaterials, which negatively affects their surface and their nanoscale properties [24]. This agglomeration of NPs can be prevented by increasing the zeta potential of the nanomaterials (increasing the repulsion force) [25], optimizing their degree of hydrophilicity/hydrophobicity or by optimizing the pH and ionic strength of the suspension medium [22]. When the investigated nanostructures have dimensions in the range of 1 - 100 nm, quantum effects become more evident. These quantum nanostructures are physical nanostructures in which subatomic particles are limited by physical dimensions. As a result of this quantum confinement effect, some non-magnetic macroscopic materials (Pd, Pt, Au) become magnetic when used as nanomaterials in various applications.

CHAPTER 2. EXPERIMENTAL METHODS

2.1 SYNTHESIS OF Pt-NPs THROUGH PULSED LASER ABLATION IN LIQUID MEDIUM

The pulsed laser ablation in liquid medium (PLAL) is a physical method, "top-down" approach, versatile and relatively simple, which can be used at room temperature without the use of an ultra-high vacuum facility. Therefore, it is an easy-to-implement technique through which clean and chemically pure NPs with different diameters can be obtained.

Pt-NPs were fabricated via the PLAL technique using the KrF excimer laser, and this experimental setup can be seen in Figure 2.1.

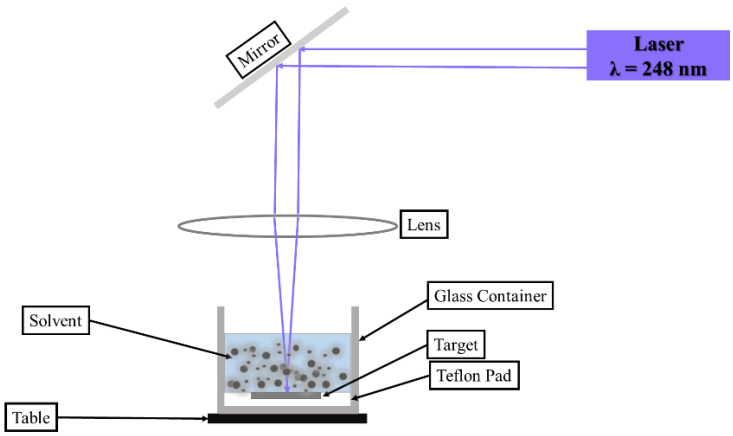

Figure 2.1. Experimental setup of the PLAL method.

As can be seen in Figure 2.1, the working principle of this method is based on the ablation of a metal target that is in a liquid medium. In other words, following the ablation process, the material is removed from the target and NPs are formed with the help of the liquid medium. Specifically, the pulsed laser beam is directed to a mirror whose role is to redirect it to the biconvex focusing lens. The latter has the role of concentrating and redirecting it so that it reaches perpendicular to the surface of the target for the ablation process to take place. The metallic target, Pt, is immersed in the liquid medium (bidistilled water, ethanol, etc.) being fixed on a Teflon support on the surface of which a shape similar to that of the target has been built to keep it fixed during the entire ablation process. The target, the Teflon support and the liquid used are in a glass beaker where the NPs ablation and acquisition process is performed.

In all experiments, the irradiation source used was the KrF COMPex Pro 205 excimer laser with a wavelength of 248 nm and a pulse duration of 20 ns, manufactured by Coherent Inc. (Santa Clara, CA, USA). The laser beam is focused using a biconvex quartz lens with a focal length of 30 cm positioned before the laser beam reaches the target surface, and the distance between the lens and the target surface was 30.4 cm. In the case of the liquid medium, bidistilled water, aqueous ethanol solution and aqueous isopropanol solution, an initial volume of 6.7 mL was used, less in the case of the ionic liquid system based on choline chloride with ethylene glycol, ChCl:EG (molar ratio of 1:2) in which a volume of 13 mL was used. Technologycal parameters such as laser fluence, repetition rate (RR), ablation time and liquid medium were optimized in order to obtain metal NPs with the smallest possible diameters. The laser fluence was varied from 2.3, 4.0 and up to 5.8 Jcm-2, the RR was modified having values of 10, 30 and 50 Hz., less in the case of ChCL:EG where RR values such as 3 were used , 5, 7 and 10 Hz. The ablation time was constant in each ablation process for the 4 liquid media. In double-distilled water ablations it was fixed at 15 minutes, in aqueous ethanol solution at 10 minutes, in aqueous isopropanol solution it was varied from 1 to 10 minutes (1, 3, 5, 7 and 10 minutes) for the 2 values of RR, 10 and 50 Hz, and in the case of ChCl:EG it was 20, 30 and 40 minutes. After obtaining these colloidal solutions, different analysis techniques were used to evaluate the properties of Pt-NPs.

2.2 STRUCTURAL AND MORPHOLOGICAL ANALYSIS TECHNIQUES

2.2.1 Ultraviolet/Visible Spectroscopy (UV/Vis)

The optical properties of the Pt-NPs samples following the PLAL process were determined by recording the transmission spectra in the wavelength range from 200 to 900 nm using a Perkin Elmer Lambda950 spectrophotometer equipped with a PbS detector with a Peltier controller having the spectral resolution of 0.05 nm in the UV/Vis range.

2.2.2 High Resolution Scanning and Transmission Electron Microscopy – Energy Dispersive X-ray Spectroscopy (HR-STEM-EDX)

The morphological properties, mean size, size distribution and internal structure, were investigated by HR-STEM using a Hitachi HD-2700 system operating at an accelerating voltage of 200 kV and equipped with the X-ray energy dispersive (EDX) having an X-max 100 TLE detector from Oxford Instruments.

2.2.3 Direct Analysis Mass Spectrometry in Real Time (DART-MS)

Direct real-time analysis ion source-equipped mass spectrometry (DART-MS) is an analytical and non-destructive technique, detecting sample-specific ions. Elemental analysis of nanoparticles was studied by AccuTOF LC—plus 4G MS from JEOL, Akishima, Japan, equipped with a DART ionization source from IonSense Inc., Saugus, MA, USA. The DART-MS system was used to confirm the presence of Pt atoms in the fabricated colloids after the completion of the laser ablation process.

2.2.4 X-Ray Diffraction (XRD)

X-ray diffraction is a non-destructive technique used in determining the type of structure and its orientation and whether the structure is crystalline or not. Additionally, different structural characteristics on the sample can be analyzed such as crystallite size, tension and stress in the material. The crystal structure of the produced Pt-NPs was determined by means of the X-ray diffraction (XRD) technique using a high-resolution X-ray diffractometer produced by Rigaku SmartLab with a CuKα radiation ($\lambda = 0.15406$ nm) in the range of 2θ from 30 to 90°.

2.2.5 Surface-Enhanced Raman Spectroscopy (SERS)

Surface-enhanced Raman spectroscopy is a non-destructive and surface-based technique by amplifying the scattering of the Raman signal using molecules that are tightly bound to the metal surface. The Raman study was performed at room temperature using a LabRam HR800 system produced by Horiba with a spectral resolution in the visible range of

0.6 cm^{-1}. The Raman spectrum was generated by exposing the sample for 25 seconds at a power of 0.8 mW with a red excitation laser having a wavelength of 632 nm at 50x magnification and scattering the signal emitted by the sample on the CCD detector using a 600 grating lines/mm. This technique was used to investigate the influence of Pt-NPs in methylene blue dye to detect the enhancement of the pigment signal in the presence of metal NPs.

2.2.6 Fourier Transform Infrared Spectroscopy (ATR-FTIR)

Fourier transform infrared spectroscopy (FTIR) is a vibrational spectroscopic method that is useful in the study of molecular bonds. ATR - FTIR spectra were recorded at room temperature using a Perkin Elmer Spectrum Two IR spectrometer. Attenuated total internal reflection FTIR measurements were performed by averaging 20 scans, with a resolution of 2 cm^{-1}, in the wavenumber range 8500 – 450 cm^{-1}.

CHAPTER 3. SYNTHESIS OF PLATINUM NANOPARTICLES USING LASER ABLATION WITH KrF EXCIMERS IN BIDISTILLED WATER

3.1. INTRODUCTION

Colloidal platinum nanoparticles (Pt-NPs) have attracted significant attention due to their physical and chemical properties, including stability, dispersion, size, shape, and morphology, which further determine their final applications, ranging from biotechnology to electronics. They may act as strong catalysts for the reduction of polluting gases generated by vehicles [1] or for the elimination of nitrous oxide generated in combustion processes [2], and they may enhance the catalytic activity for oxygen reduction reactions during the operation of proton exchange membrane fuel cells [1,3]. They have important applications in oxygen reduction reactions (ORRs) due to their remarkable electrocatalytic characteristics [4]. These reactions play a significant role in corrosion [5], water electrolysis [6], electrochemical energy conversion [7], diverse industrial processes [8], etc.

Two parameters of the Pt-NPs synthesis route were varied in order to optimize their characteristics: the laser fluence and the RR. Pt-NPs samples were produced under constant laser fluences of 2.3, 4.0, and 5.8 J cm^{-2} for 5 different RRs of 10, 20, 30, 40 and 50 Hz, respectively.

3.1. The effect of RR on the synthesis of Pt-NPs when the laser fluence is constant

The UV/Vis transmission spectra of the samples obtained at constant laser fluence of 2.3 Jcm^{-2} but varying the RR values (from 10 to 50 Hz) during the laser ablation process are represented in Figure 3.3.

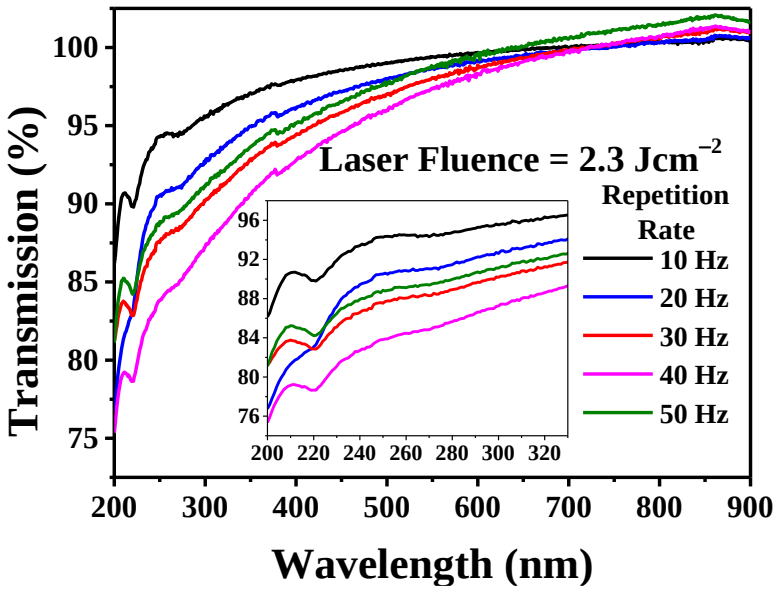

Figure 3.3. UV/Vis transmission spectra of Pt-NPs prepared at laser fluence of 2.3 Jcm^{-2} and different RR: 10, 20, 30, 40 and 50 Hz.

As can be noted in Figure 3.3, the optical transmission of Pt-NPs obtained at 10 Hz has the highest transmission values around 95% in the whole wavelengths range, and the colloidal solution prepared at 40 Hz has the lowest transmission values. It can be seen that when RR increases from 10 Hz to 40 Hz, the optical transmission values decrease from 95% up to 78%. This is due to the amount of ablated material obtained in the final colloid. But in the case of Pt-NPs manufactured at 50 Hz, this behavior is no longer valid, the transmission of the colloid being higher than 30 and 40 Hz. It is considered that in the case of this solution a more pronounced phenomenon occurred than in the other samples, namely the occurrence of optical discharge due to the high value of the repetition rate and the volume lost following the PLAL process. As mentioned above, this sample was considered to observe the growth evolution of Pt-NPs with RR amplification.

By using the HR - STEM imaging technique, Figure 3.5 shows the morphological characteristics of the samples fabricated at a constant fluence of 2.3 Jcm^{-2} but at different values of RR from 10 Hz (Fig. 3.5 I), 20 Hz (Fig. 3.5 II), 30 Hz (Fig. 3.5 III), 40 Hz (Fig. 3.5 IIV)

and up to 50 Hz (Fig. 3.5 V). Due to a special feature of the technique, ZC - atomic mass phase contrast (Figure 3.5a) and transmission (Figure 3.5b) images were acquired simultaneously at the same magnification (x500K) and at the same location on the sample for each sample, also called co-located images.

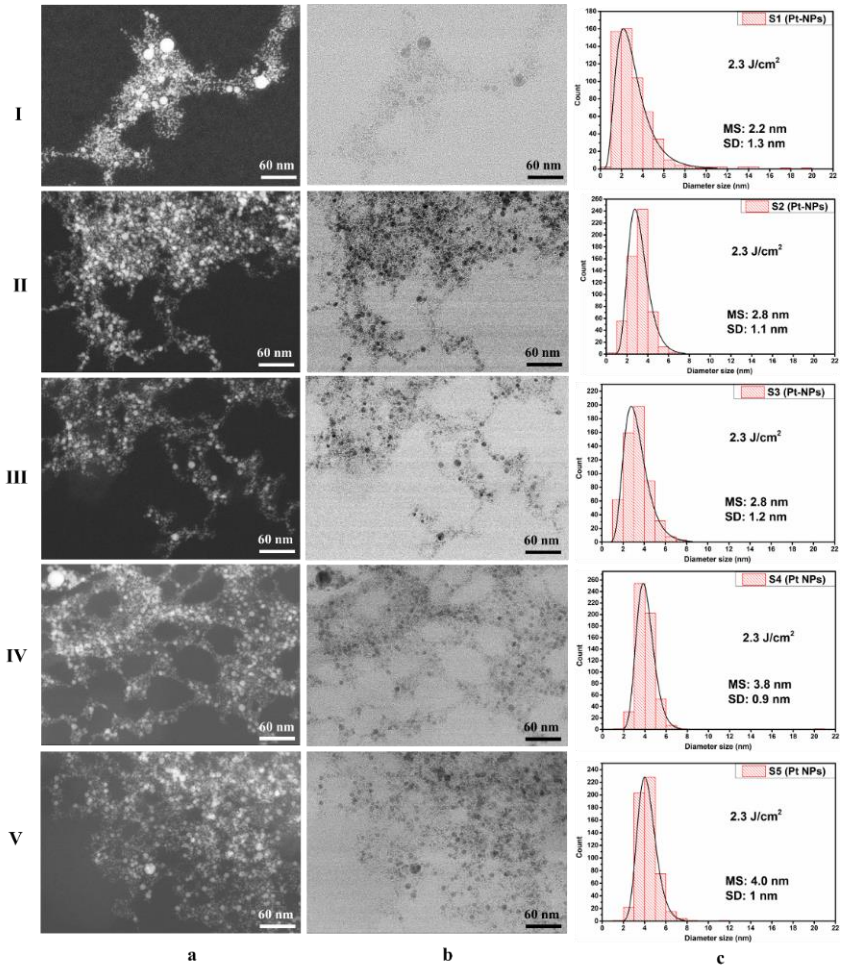

Figure 3.5. Pt-NPs synthesized at a laser fluence of 2.3 Jcm^{-2}: a) ZC images; b) TEM images; c) distribution of corresponding sizes for different RR: I) P1 (10 Hz), II) P2 (20 Hz), III) P3 (30 Hz), IV) P4 (40 Hz) and V) P5 (50 Hz).

HR-STEM images showed that the Pt-NPs mainly exhibit a spherical and spherical-like shape, and many agglomerates and very small NPs are also present. In order to have good statistics, 550 individual Pt-NPs were measured by means of ImageJ software, and their histograms were fitted with lognormal distribution.

The lowest value of the average size of 2.2 nm was determined in the case of Pt-NPs obtained at 10 Hz RR, as can be seen in Figure 3.5 (I-c). For the colloid fabricated using the

RR value of 20 Hz, the average diameter value increases to 2.8 nm (see Figure 3.5 (II-c)). In the case of NPs manufactured at 30 Hz, the average diameter value remains the same as can be seen in Figure 3.5 (III-c). However, for the colloids obtained at 40 and 50 Hz, the values of the average diameters of Pt-NPs increase up to 3.8 nm and 4.0 nm, respectively, as can also be noted in Figure 3.5 (IV-c, V-c).

An increase in mean size from 2.2 to 4.0 nm was observed. In Figure 3.6, the graph between the average diameter of Pt-NPs versus RR at the laser fluence of 2.3 Jcm^{-2} is represented.

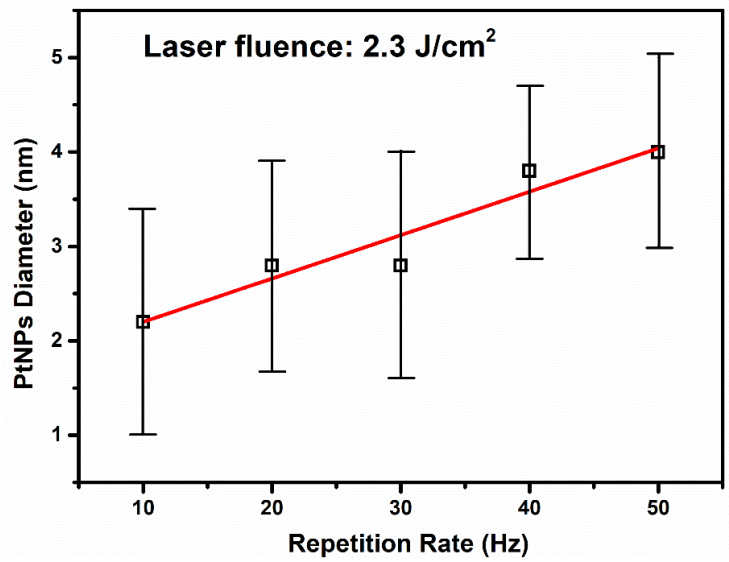

Figura 3.6. Diametrul mediu al Pt-NPs crește liniar cu RR.

Such a linear dependence is confirmed by previous works on Au-NPs and Ag-NPs [62,63]. However, this is the first report of the synthesis of Pt-NPs using a KrF excimer laser as the irradiation source.

3.3. HR-STEM investigation for Pt-NPs

HR-STEM images of individual Pt-NPs, acquired at x8000K magnification (Figure 3.17a), demonstrate the attainment of spherical shape, crystallinity and fully metallic nature of the NPs. By using such images, the profiles corresponding to the interplanar distance values were measured for the investigated samples, P1 and P11 (see Figure 3.17b). So, the interplanar distances of 0.22 nm and 0.23 nm (Figure 3.17b) for the crystal planes of Pt (111) were obtained from the red squares drawn in the images obtained with the transmitted electrons (Figure 3.17a). These values are almost identical to the ideal value of 0.23 nm for platinum crystalline material with an FCC type structure [65-69].

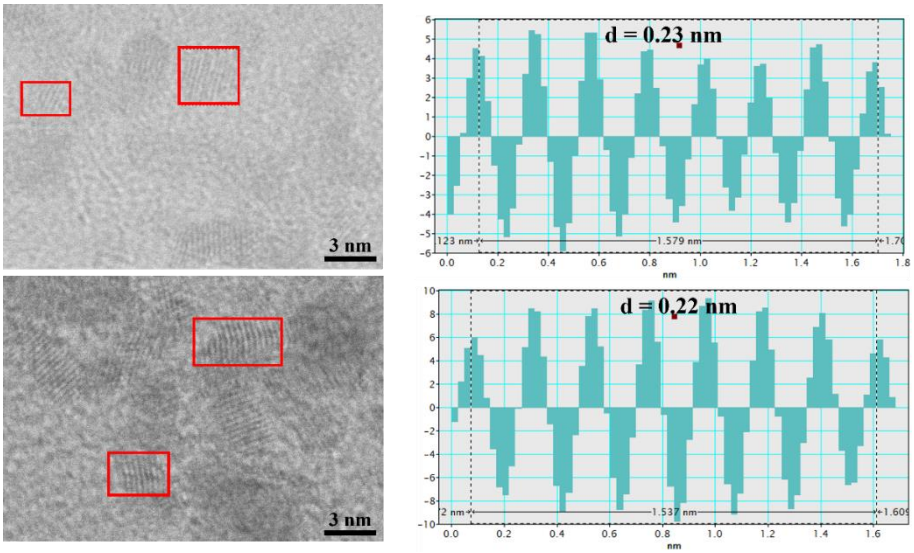

(**a**) (**b**)

Figure 3.17. a) HR-STEM image of Pt-NPs colloids fabricated at 10 Hz RR for P1 and P11; b) the corresponding profile for measuring the inter-planar distance.

3.4. Confirmation of the Pt presence in the final solution

EDX analyzes performed on sample P1 in the same position as TEM analysis (Figure 3.18 (I- a)) confirm that the nature of the NPs in the colloids is Pt. The EDX technique is useful to identify the elemental composition of the investigated sample. EDX mapping of Pt-NPs is shown in Figure 3.18 - left side, and the distribution of Pt-NPs on the Au grid can be seen in yellow color. Since there is a thin layer of carbon on the surface of the Au grid to support the investigated sample (Pt-NPs), the distribution of carbon is also observed in red.

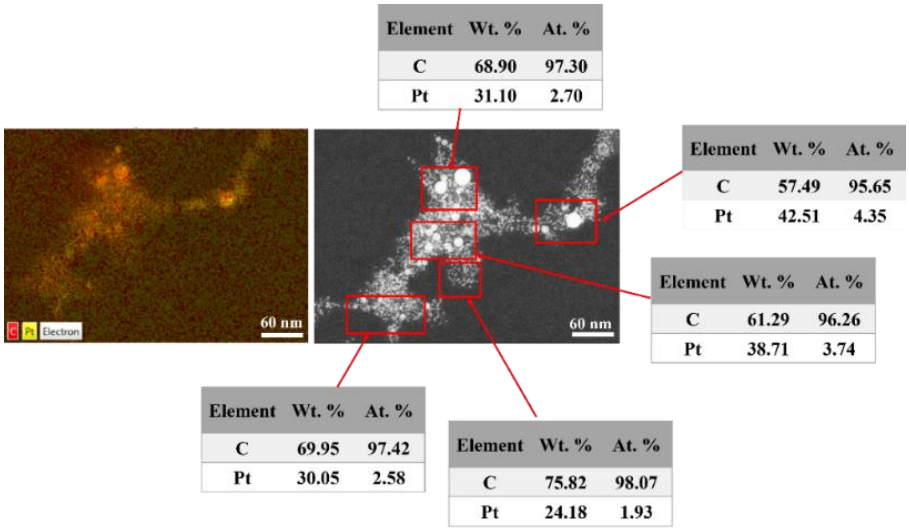

Figure 3.18. EDX analysis of Pt-NPs acquired at x500K magnification: mapping analysis (left side) and elemental composition analysis (right side).

The elemental composition of the samples in atomic and mass percentages was determined from the EDX spectra corresponding to the areas indicated by red rectangles as shown in Figure 3.18 - right side. The average mass percentage of Pt-NPs was found to be around 33.31%, and the remaining 66.69% was attributed to the carbon material. The average atomic percentage of Pt-NPs was determined to be 3.06% and the remaining 96.94% for carbon.

It is worth mentioning that EDX analysis was performed for NPs with the smallest average diameter (2.2 nm) confirming the presence of Pt in the colloids. DART - MS is a very sensitive tool to search for the presence of a specific atomic mass in the sample and has been involved as a complementary technique.

MS equipped with a DART source was used without any further preparation of the solution, and the presence of Pt was confirmed by a direct analysis of the final solution obtained.

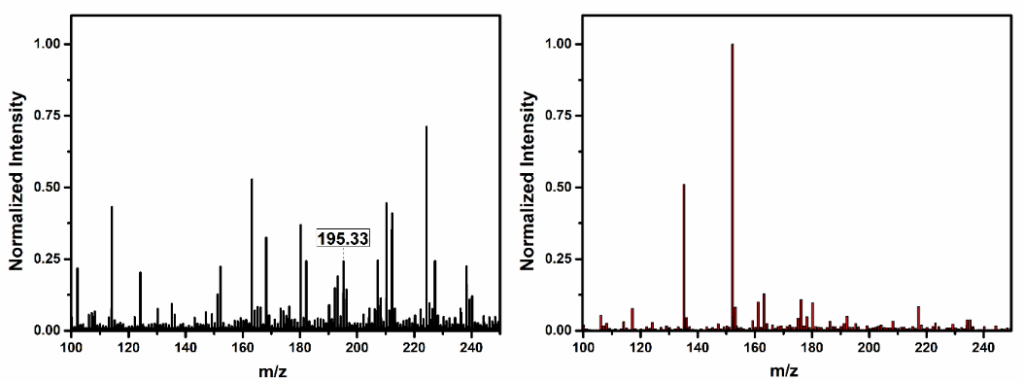

(**a**) (**b**)

Figure 3.19. DART - MS spectra: a) spectrum of Pt-NPs colloidal solution b) spectrum for DDW.

The DART-MS spectrum of the investigated sample shows a visible line at 195.33 u. (Figure 3.19a) corresponding to the atomic mass of platinum (the standard atomic mass for Pt is 195.09 u.). On the other hand, the platinum line is missing in the spectrum of bidistilled water in Figure 3.19b before the ablation process. This is direct evidence for the presence of Pt in the colloidal solution, which is also supported by measurements of the platinum crystal lattice with HR-STEM and EDX analysis.

CHAPTER 4. FABRICATION OF Pt NANOPARTICLES BY PULSED LASER ABLATION IN AQUEOUS ETHANOL SOLUTION USING A KrF EXCIMER LASER

In Chapter 4, a new solvent, namely, ethanol aqueous solution, was used, and three parameters of the synthesis method to obtain Pt-NPs were varied to adjust their characteristics: laser fluence, RR, and ethanol concentration. Pt-NPs samples were produced under constant laser fluences of 2.3, 4.0 and 5.8 Jcm^{-2} for three different RR values of 10, 30 and 50 Hz, using ethanol concentrations of 10, 20, 40, 60, 80 up to 100 %, keeping constant the ablation time (10 minutes) and the volume of solvent used (6.7 mL).

4.3.3. The influence of ethanol concentration

The comparison between the optical transmission spectra of the produced colloids is shown in Figure 4.14. Furthermore, two UV/Vis spectra are shown, 4.14-a includes the data

obtained when the spectrum was recorded using the initial ethanol concentration before ablation as a reference solution, and another, Figure 4.14-b, contains the data obtained with the ethanol concentration calculated after the completion of the ablation process determined using Equation (4.14). On the one hand, without correction, a band in the 200-220 nm range appeared in Figure 4.14-a. The transmission values of this band decrease with increasing ethanol concentration. When ethanol concentration above 60% is used, the effect commented above is more pronounced. On the other hand, when the calculated ethanol concentration is used as a reference, Figure 4.14-b, this band is not observed, highlighting the influence of the evaporated ethanol concentration in the UV/Vis spectra. In the rest of the discussion, we will focus on the corrected spectra of Figure 4.14-b. The transmission band between 230 nm and 340 nm is attributed to the surface plasmon resonance in the case of Pt-NPs. The band minimum position oscillates with increasing ethanol concentration. Throughout the measured range, the optical transmission values of the corresponding spectra decrease with increasing concentration of the volatile component in the solution.

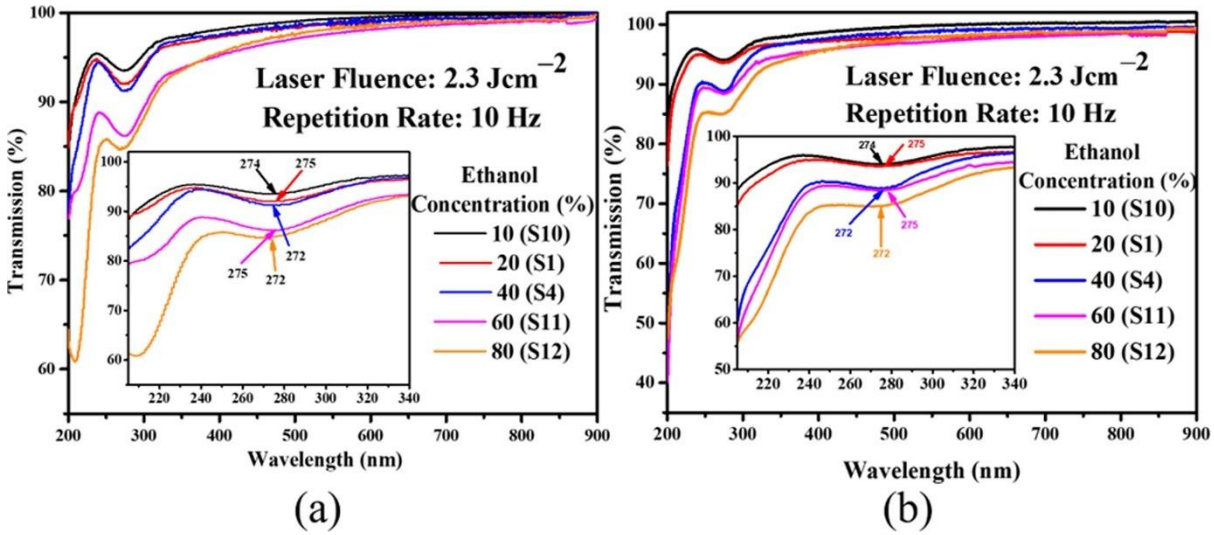

Figure 4.14. Optical transmission spectra of Pt-NPs fabricated at different ethanol concentrations (10, 20, 40, 60 and 80%), laser fluence (2.3 Jcm^{-2}) and 10 Hz: a) uncorrected and b) corrected. The inset figure is a magnification in the 205-340 nm range.

The morphological characterization of Pt-NPs by HR-STEM is shown in Figure 4.16 from I to V (a, b) and the corresponding size distributions are shown in Figure 4.16-c.

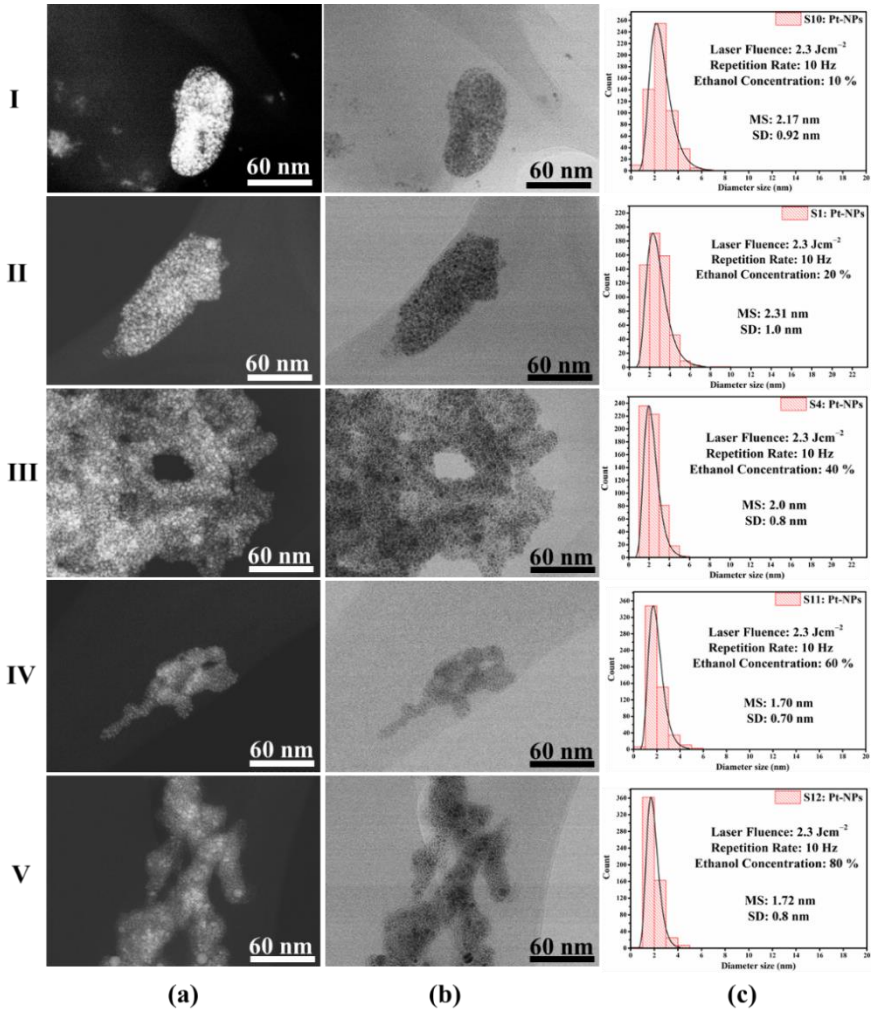

Figure 4.16. Co-localized HR-STEM images for Pt-NPs obtained at constant value for RR of 10 Hz and a laser fluence of 2.3 Jcm^{-2}, but different concentrations of ethanol (10 % - I, 20 % - II, 40 % - III , 60% - IV and 80% - V): a) ZC images, b) TEM images and c) the corresponding histograms.

As can be seen from all the images (Figure 4.16 I-V-a, b) a high level of agglomeration is presented in the investigated colloids. The characteristic size of the aggregates increases slowly with increasing ethanol concentration from 10% to 40%, the largest being observed at 40%. Further increase in ethanol concentration up to 60% leads to a rapid decrease in aggregate size, while at 80% ethanol concentration it became larger again. When varying the ethanol concentration from 10% to 60%, the average diameter of NPs decreases from 2.17 ± 0.92 nm to 1.7 ± 0.7 nm. A further increase of up to 80% does not affect the mean diameter. The sizes of the NPs are distributed in the range of 1-8 nm. The values of the average diameter obtained in the case of Pt-NPs produced with a laser fluence of 2.3 Jcm^{-2} allow us to assume an approximate linear dependence on the ethanol concentration, which is presented in Figure 4.16. In general, it can be seen that the average diameter of NPs decreases with increasing ethanol

concentration. A possible explanation for this behavior could be that with increasing ethanol concentration, the laser energy absorption increases (Figure 4.16), which means that the laser fluence value decreases when it hits the target surface, as commented above. Consequently, the amount of ablated material should be reduced, and this leads to the synthesis of smaller NPs.

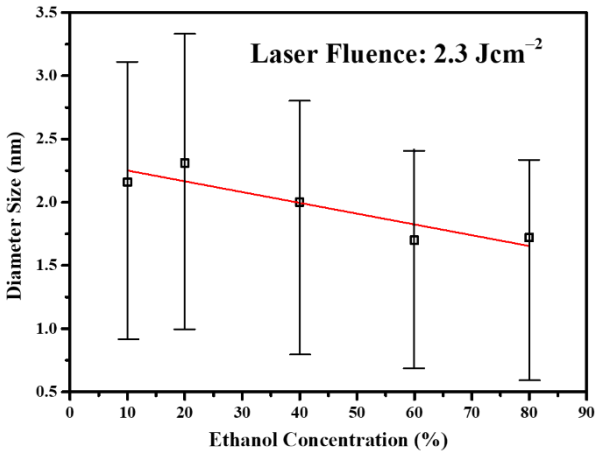

Figure 4.16. The linear dependence of the size of the mean diameters of Pt-NPs obtained at constant parameters, RR of 10 Hz and laser fluence of 2.3 Jcm^{-2}, against ethanol concentrations (10 - 80 %).

The diffractogram obtained after the XRD analysis of Pt-NPs on Si substrate is shown in Figure 4.19-a. The diffraction peaks at 2θ = 39.9, 46.4 and 81.7 ° correspond to the indexed crystal planes of platinum (111), (200) and (311), respectively (card No. 1011107), confirming the formation of Pt-NPs with a cubic structure with face centered (FCC) [46-48]. The X-ray diffraction pattern of the NPs matched that of the Pt target used in the nanomaterial synthesis, as can be seen in Figure 4.19-b [49]. The interplanar distance (d) from the XRD analysis is 0.25, 0.19 and 0.12 for the crystal planes of Pt (111), (200) and (311), respectively. Therefore, the results obtained from the XRD analysis are in good agreement with those from the HR-STEM analysis.

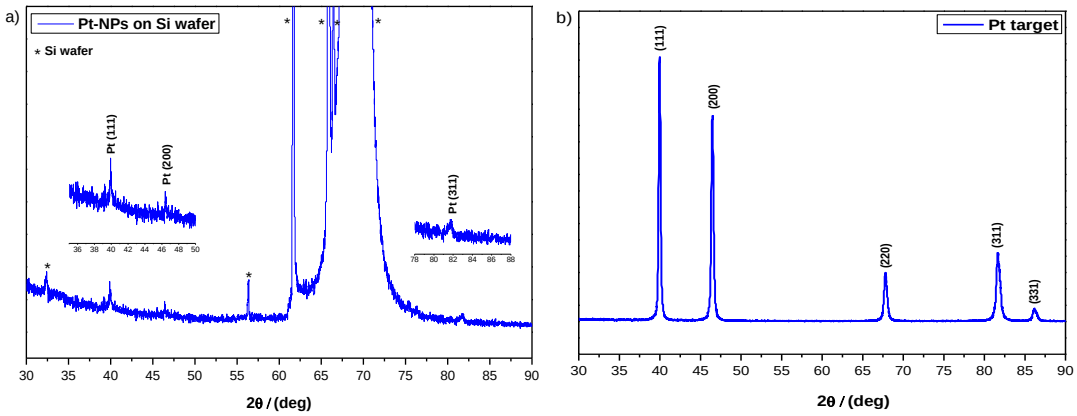

Figure 4.19. X-ray diffractogram of: a) Pt-NPs deposited on Si substrate and b) Pt target.

4.3.4. The aplicability of Pt-NPs in SERS analysis

Even though noble metals such as Pt have been considered inactive for surface-enhanced Raman spectroscopy (SERS), several groups have demonstrated the use of Pt structures as active SERS substrates [12,13]. In this work, we explore the scattering contribution of synthesized Pt-NPs in the detection of methylene blue (MB). MB is an antifungal dye used in aquaculture due to its ability to prevent fish diseases. The Raman spectra of the dry solution of MB are shown in Figure 4.21, with the main peaks at 446 and 1625 cm^{-1}, attributed to C-N-C bonding and C-C stretching modes, respectively. As can be seen, the characteristic bands of the dye are weak and hard to see. In the same figure, in red color, the spectrum of the dry solution of MB with Pt-NPs, synthesized at a laser fluence of 2.3 Jcm^{-2} and RR of 50 Hz in aqueous solution with ethanol concentration of 80 %, is shown. The peaks for MB became very intense, due to the activity of Pt-NPs. The characteristic peaks of the dye show a small shift at 448 and 1627 cm^{-1}. Considering the band around 1627 cm^{-1}, the ratio of its intensity for MB adsorbed with and without SERS substrate, respectively (I_{SERS} / I_{Ref}) is 14.8, indicating a signal increase of more than an order of magnitude.

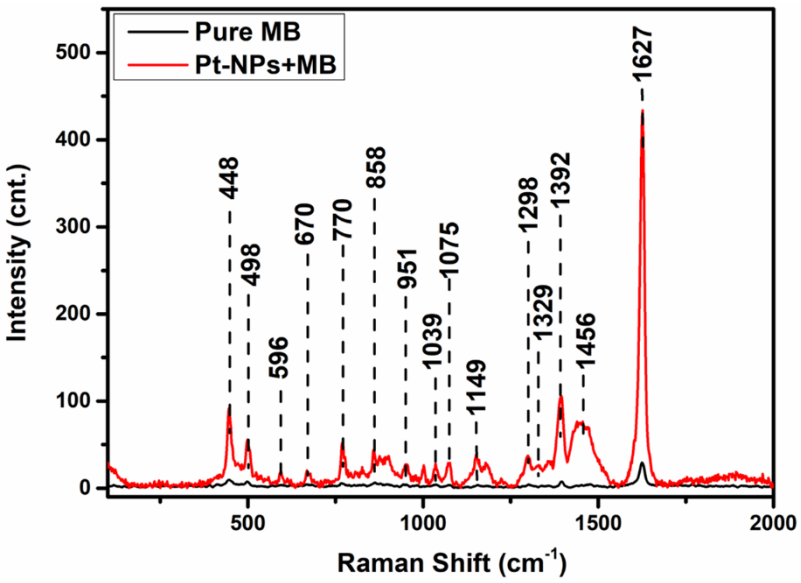

Figure 4.21. Raman spectra of MB dye (black curve) and Pt-NPs - MB colloid (red curve).

CAPITOLUL 5. SINTEZA DE Pt-NPs ÎN SOLUȚIE DE IZOPROPANOL CU LASERUL CU EXCIMERI KrF ȘI UTILIZAREA LOR ÎN SERS

In chapter 5, a liquid medium from the same range of alcohol-based solvents, aqueous isopropanol solution was introduced and four parameters of the synthesis method to obtain Pt-NPs were varied to adjust their optical and morphological properties: laser fluence, RR, ablation time and isopropanol concentration. Pt-NPs samples were produced under constant laser fluences of 2.3, 4.0 and 5.8 Jcm^{-2} for three different RR values of 10, 30 and 50 Hz in different isopropanol concentrations from 10, 20, 30, 40, 60 , 80 to 100 %, varying the ablation time (1, 3, 5, 7 and 10 minutes) but keeping the solvent volume constant (6.7 mL).

5.3.1. The importance of isopropanol concentration on the synthesis of Pt-NPs

A series of experiments were performed to study the influence of different concentrations in the aqueous isopropanol solution used as the liquid medium in the PLAL method. The concentrations of isopropanol included in the experiment were - 10, 20, 30, 40, 60, 80 and 100 %, respectively. By measuring the colloids obtained as a result of the ablation, the UV/Vis spectra of the Pt-NPs were determined, which are shown in Figure 5.6-a. It is relevant to emphasize that a reference solution with the appropriate starting concentration of isopropanol was used to obtain each spectrum. The other technological parameters used to

make this series have the same values for all samples, laser fluence of 2.3 Jcm^{-2}, RR of 10 Hz and ablation time of 10 min. The values of all spectra in the region above 340 nm are approximately the same. Below this value the differences between the spectra become apparent. In all spectra there is the well-known plasmonic band with limits between about 240 nm and 340 nm. The width is unchanged for individual samples. The position of its minimum is sequentially slightly red-shifted from 269 nm for sample P1 (10% isopropanol) to 275 nm for P7 (100% isopropanol). In some of the spectra, exactly at - 40, 60, 80 and 100 %, a second band appears. A feature that indicates that the measurement spectra can be considered unreliable is in the range between 200 and 220 nm, where the transmission values are above 100 %, close to 160 % for an isopropanol concentration of 80 %. Therefore, to obtain real UV/Vis spectra, the reference liquid should be changed. Instead of a solution with an initial concentration of isopropanol, one with a concentration calculated according to the procedure described above in equation (5.1) is used. The resulting spectra are shown in Figure 5.6 (b). The commented procedure overcomes the main drawback of the original procedure of obtaining UV/Vis spectra expressed in the presence of transmission values exceeding 100 %. This fact makes the corrected spectra more real and justifies their further use as a basis for the analysis of the obtained Pt-NPs properties, see Figure 5.6-b.

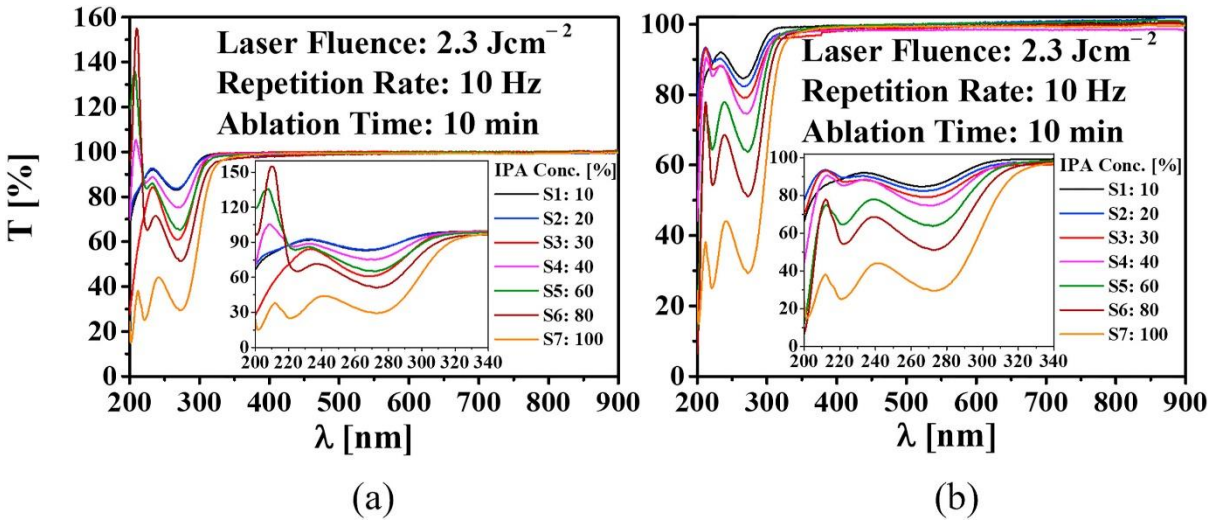

Figure 5.6. UV/Vis optical spectra of Pt-NPs fabricated with 2.3 Jcm^{-2} and 10 Hz RR for 10 min in different concentrations of isopropanol (10 % - 100 %.): (a) spectra acquired with initial concentrations and (b) corresponding spectra with concentrations calculated using equation (5.1).

The electronic HR-STEM images obtained on Pt-NPs fabricated with lower and constant values of laser fluence (2.3 Jcm^{-2}) and RR (10 Hz) but with variable concentration of

isopropanol in the range from 10 to 100 % are presented in Figure 5.8 I-VII. Two different types of images were applied namely, ZC - phase contrast image shown in Figure 5.8 (a) and TEM images as can be seen in Figure 5.8 (b).

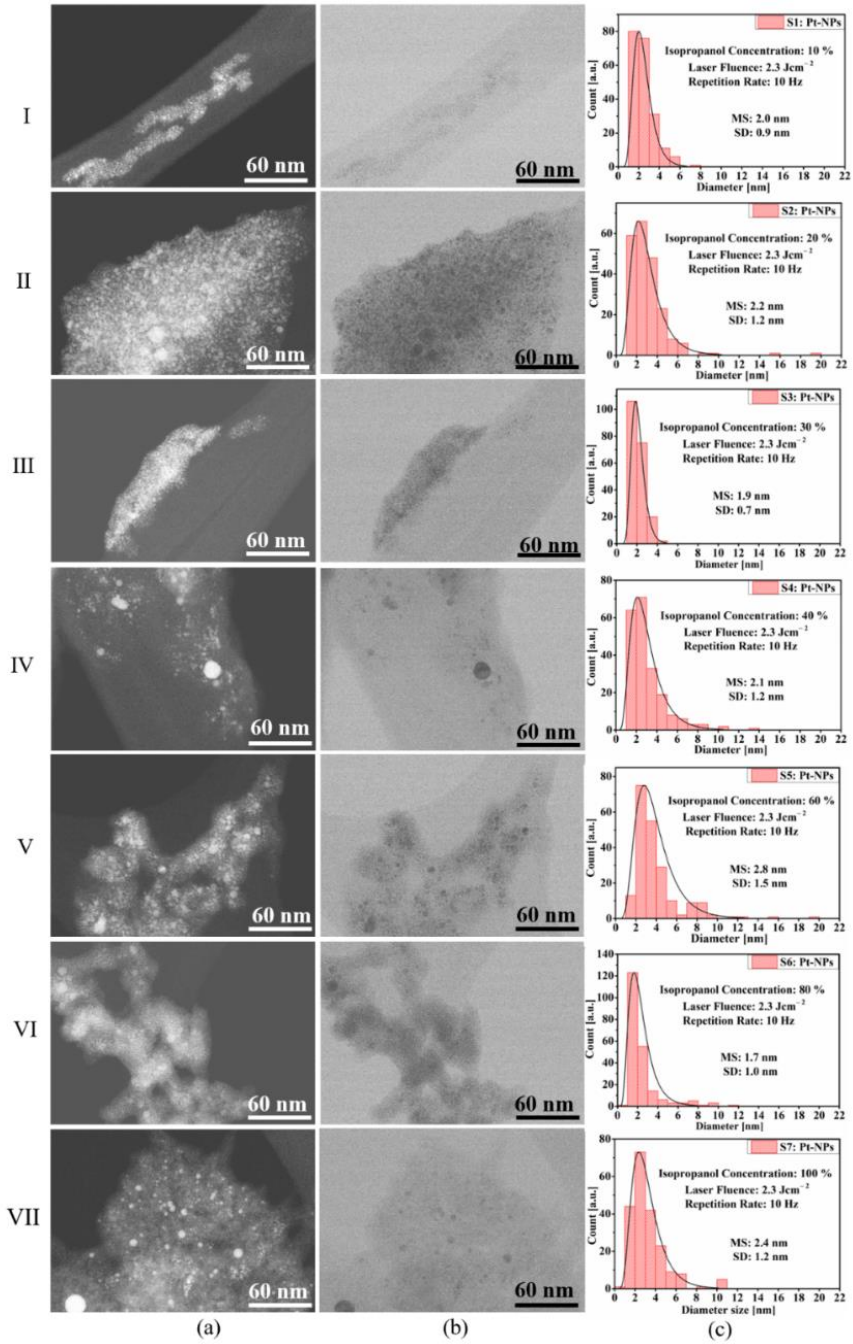

Figure 5.8. HR-STEM images of Pt-NPs fabricated with low laser fluence and RR values in different isopropanol concentrations (10 - 100 %): (a) ZC images, (b) TEM images and (c) correlated histograms.

HR-STEM micrographs presented above, Figure 5.8 (a) and (b), show the formation of aggregates with sizes in the micron range formed by very small spherical nanoparticles. It is

difficult to determine any dependence of the shape and size of the aggregates on the IPA concentration. As a general impression, aggregates formed in colloids with lower initial IPA concentration appear more compact, while those at higher concentration are more branched excepted S1 and S7 samples where the behavior is opposite. The dependence on the initial IPA concentration of the MS and the SD values of Pt–NPs does not show any definite trend. The MS values oscillate starting from 2.0 nm at 10% IPA concentration, reaching a maximum of 2.8 nm at 60% and again decreasing to 2.4 nm at 100% IPA concentration. The smallest MS value of 1.7 nm is obtained at 80% IPA concentration. The SD value of 0.9 nm at 10% IPA concentration, shows a maximum value of 1.5 nm at 60% and decreases to 1.2 nm at 100% IPA solution. The lowest value of 0.7 nm for SD is reached when 30% initial IPA concentration is used.

5.3.4. Application of the fabricated Pt-NPs

Despite the noble metals Pt–NPs were taken into account as inactive for SERS method, more investigators reported the employment of Pt material as SERS working substrates [31-33]. However, E. Kammer and co-workers involved Pt–NPs having diameters from 29 nm up to 107 nm in order to detect melamine and an increase in SERS activity was observed when 29 nm diameters Pt–NPs were used [34]. In this section, the active role of the Pt–NPs in MB detection was studied.

In this section, the active role of Pt-NPs in the detection of methylene blue was studied. Figure 5.18 shows the Raman spectra of both investigated samples, pure methylene blue (black spectrum) and small Pt-NPs with an average diameter of 1.72 nm, fabricated with laser fluence (2.3 Jcm^{-2}), 10 Hz for 10 minutes in isopropanol concentration of 80% (red spectrum) aqueous solution which was mixed with pure methylene blue and dried on a glass slide. Raman peaks located near 466 cm^{-1} and 1625 cm^{-1} were assigned to C-N-C (skeletal bending) and C-C stretching modes. As can be observed in Figure 5.18 - the black spectrum, the specific bands of the pigment have very low intensities and are difficult to observe. The MB peak intensities became strongly pronounced while involving Pt-NPs, because of the Pt–NPs activity in the pigment.

The MB peak shows a significant shift to 1603 cm^{-1}, while the peak characteristic for to C–N–C skeletal mode (466 cm^{-1}) has the same low intensity. It should be remarkable that the high intensity of the peak located at 1002 cm^{-1} appears in the mixed solution which can be

attributed to C–H bending mode whose initial position at 945 cm−1 in the pure MB spectrum cannot be clearly observed. Therefore, the proportion between the intensities for MB absorbed in the presence or in the absence of substrate, respectively (I_{SERS}/ I_{Ref}) is 427.24 for the peak with the highest intensity located at 1002 cm^{-1}, while the obtained value of 14.71 is for the main characteristic peak positioned at 1625 cm^{-1}. The obtained results indicate a high increase of the signal of over one order of magnitude. This behavior can occur when the MB molecules are chemically connected on the NPs surface changing the bonding energy of the pigment or it possible to be caused by a non-uniform droplet evaporation [61].

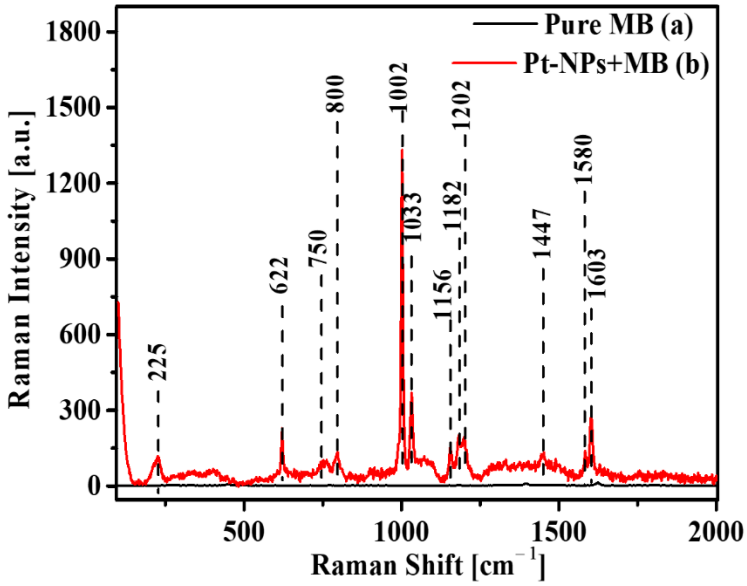

Figure 5.18. Raman spectra on pure methylene blue (black profile - a) and mixed solution between Pt-NPs and methylene blue (red - b).

CHAPTER 6. FABRICATION OF Pt NANOPARTICLES BY PULSE LASER ABLATION WITH A KrF EXCIMER LASER IN A EUTECTIC SOLVENT BASED ON CHOLINE CHLORIDE

A different solvent was used in Chapter 6, a eutectic solvent based on choline chloride and ethylene glycol in a 1:2 molar ratio and its aqueous solution with ethanol in a 1:3 volume ratio. Two parameters of the synthesis method to obtain Pt-NPs were varied in order to adjust the optical and morphological properties: laser fluence, RR and ablation time. Pt-NPs samples were produced under constant laser fluence of 2.3 Jcm^{-2} for four different RR values (3, 5, 7

and 10 Hz) varying the ablation time (20, 30 and 40 minutes) but keeping the volume constant initially of the liquid medium (13 mL).

6.3.2. Study of the dependence of the characteristics of Pt-NPs on the laser repetition rate (RR)

a) Pure ILEG

In Figure 6.4 are presented the optical transmission spectra of a series of colloids produced by PLAL in pure ILEG as liquid medium with the same laser fluence of 2.3 Jcm^{-2}, 40 min ablation time and at different values of the repetition rate 3, 5, 7 and 10 Hz, respectively (for reference liquid is used pure ILEG). As a general trend, when we compare the spectra between them, there is a decrease in transmittance values throughout the whole measurement interval with increasing of the repetition rate. This is explained by the increased transfer of energy from the laser beam to the target and the correspondingly increased amount of ablated material. In each individual spectrum one can notice the presence of three distinct bands with reduced transmission values relative to the regions in their immediate vicinity. The first of them is roughly bounded from the short-wavelength end of the measured range to about 220 nm with a minimum at about 205 nm, but with varying positions in each spectrum. The second band is located in the approximate range of 230 nm to 250 nm with a minimum around 240 nm in the spectrum of the Pt-NPs ablated at RR of 3 Hz while for the other spectra this band is so weak pronounced that it is difficult to confirm their presence at all. The boundaries of the third band are between around 247 nm – 350 nm with a minimum at about 290 nm. It should be noted that while the band boundaries of this band are different, the position of the minimum is almost the same.

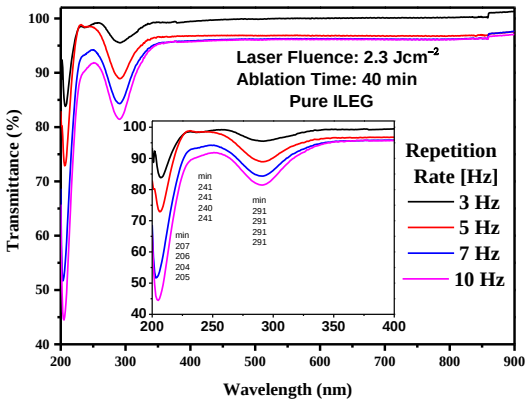

Figure 6.4. Optical transmission spectra produced with 2.3 Jcm^{-2} for an ablation time of 40 minutes at different repetition rate values - 3, 5, 7 and 10 Hz, respectively.

The morphological properties of the considered samples were investigated through HR-STEM measurements and the results are presented in Figure 6.6 (I-IV). The ZC and TEM images are shown in Fig. 6.6a, b and the corresponding histograms (Fig. 6.6c) were compiled in order to determine the size distribution and the mean size values.

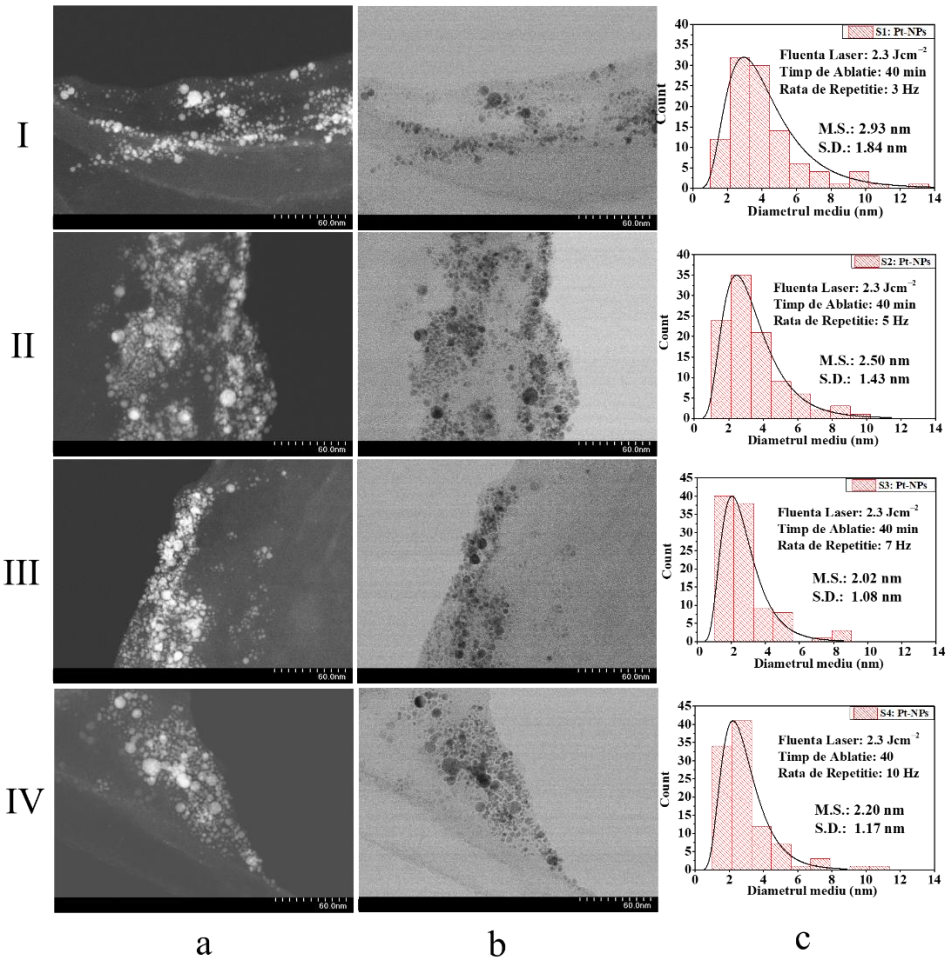

Figure 6.6. Co-localized HR-STEM images for Pt-NPs colloids obtained in pure ILEG at constant laser fluence of 2.3 Jcm^{-2} ablation time of 40 minutes at four different values of RR – 3, 5, 7 and 10 Hz, respectively : a) ZC images, b) TEM images and c) corresponding size distributions.

As can be seen from co-localized images (ZC – fig. 6.6a, TEM – fig. 6.6b) the shape of the synthesized Pt-NPs is predominantly spherical, the aggregation level is relatively low, and they are mainly separated in all samples.

In this series the Pt-NPs prepared with 7 Hz RR show the smallest mean size value of 2.20 ± 1.20 nm, while the biggest NPs of 2.79 ± 1.60 nm mean size were obtained by applying

3 Hz RR. In our opinion, this could be attributed to manifestation of the photofragmentation effect.

b) solution of ILEG with ethanol (1:3)

In Figure 6.7 are displayed the optical transmission spectra of four ensembles of Pt-NPs synthesized by PLAL in a solution of 1:3 ratio of ILEG and pure ethanol (99.9 %). The UV/Vis spectra were acquired using as references the final concentrations of the colloids according to Table 1. The four colloids are fabricated with 3, 5, 7 and 10 Hz, respectively, and the same other technological parameters – 2.3 Jcm-2 laser fluence and 40 min ablation time. In all four spectra of Pt-NPs created with a 3, 5, 7 and 10 Hz RR, the plasmon bands minimum around 290 nm is very weak pronounced and their positions are hard to be determined. The same is established for the band with a minimum located at 240 nm whereby is hard to say if it exists at all. The minimum of the band hypothesized to be due to an interband transition at about 202 nm is clearly pronounced in all four spectra. The three spectra of the Pt-NPs synthesized with 3 – 7 Hz RR are near parallel to each other. It shows that changes of the repetition rate in this interval hardly affects the ablation process with the chosen solution. For the Pt-NPs created with the highest RR of 10 Hz the transmission values in almost the entire measured range of wavelengths are lower than their corresponding values in the other three spectra. This is related to the increased amount of ablated material associated with the increased energy exchange between the laser beam and the target. The degree of manifestation of the two bands around 202 nm and 240 nm, respectively, is preserved. However, in the range from about 250 nm to about 320 nm is clearly visible a wide structureless band assigned to the characteristic band for the surface plasmon resonance of Pt-NPs.

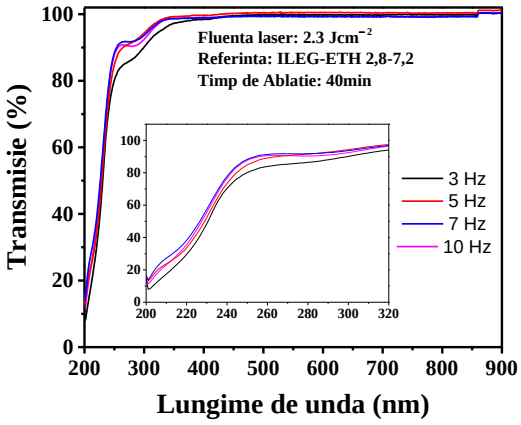

Figure 6.7. UV/Vis optical spectra of the Pt-NPs produced by PLAL in ILEG and ethanol solution (1:3) with four different repetition rate values – 3, 5, 7 and 10 Hz, respectively.

Figure 6.9 (I-IV) represents the results obtained using HR-STEM analysis in order to determine the morphological characteristics of Pt-NPs. The co-localised images are organised in the same manner as in the previous case when the liquid medium was pure ILEG (ZC and TE – Fig. 6.9 a,b, and the corresponding histograms are presented in Fig. 6.9c).

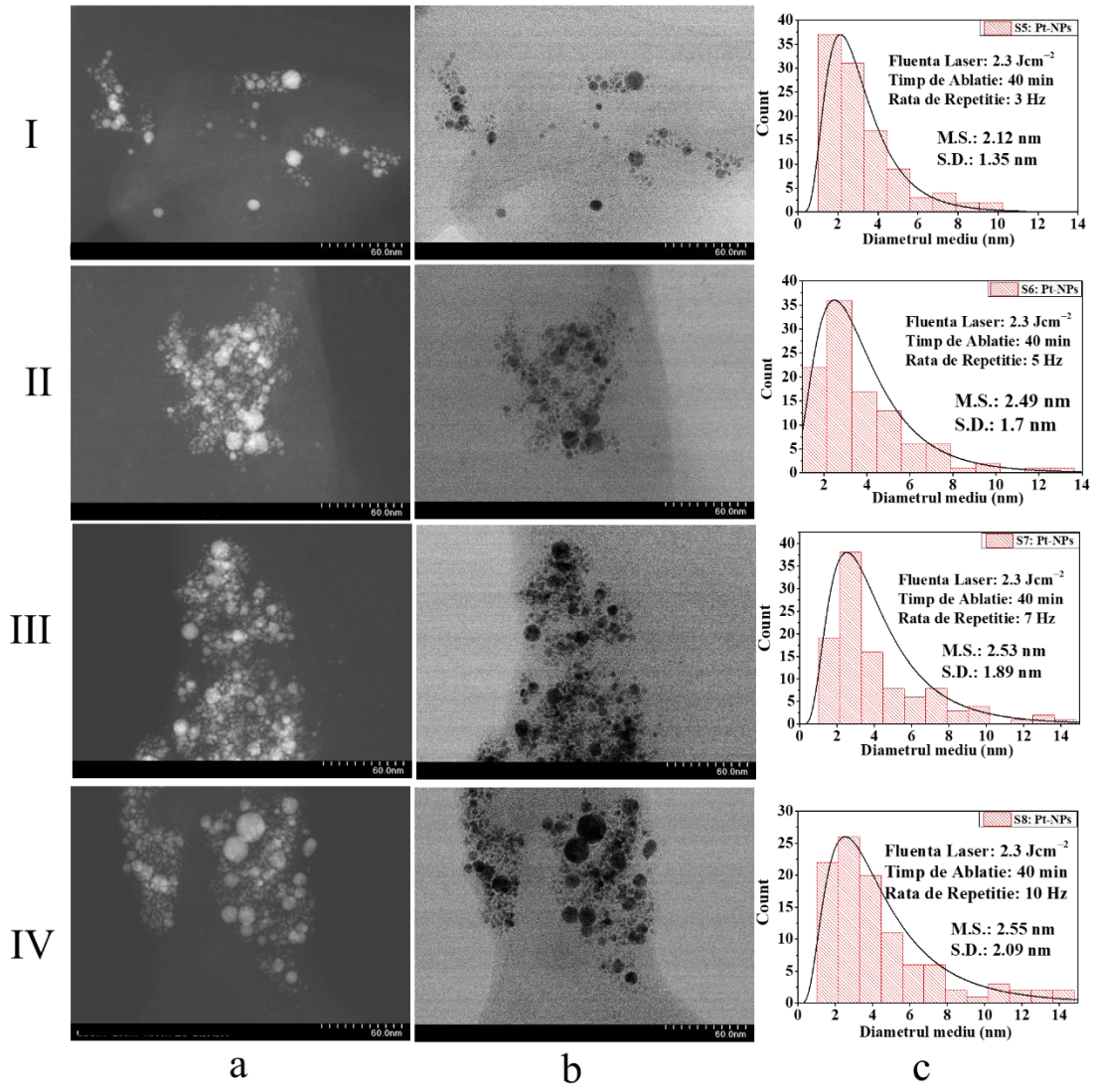

Figure 6.9. Co-localized HR-STEM images for Pt-NPs obtained in ILEG and ethanol solution (1:3) at a constant laser fluence of 2.3 Jcm^{-2}, ablation time of 40 minutes and four different values of RR – 3, 5, 7 and 10 Hz respectively: a) ZC images, b) TEM images and c) corresponding diameter distributions.

As can be seen from the above images (ZC – fig. 6.9a, TEM – fig. 6.9b) no different shape from the spherical one can be observed and the aggregation level is relatively low. The smallest mean size value of 2.60 ± 1.54 nm is obtained for the Pt-NPs prepared with RR of 3 Hz, while the biggest NPs of 2.95 ± 1.80 nm mean size were achieved for ones fabricated with 5 Hz RR. In our opinion, the enhanced quantity of ablated material raises the probability of building larger Pt-NPs but also the probability for photofragmentation. The two processes compete, and which of them prevails could be established by experiment.

3.6 Dtermination of solvent degradation

FTIR spectroscopy was applied to establish suspected changes in ILEG after its irradiation during the ablation process. In Figure 6.19 are presented two spectra of ILEG before the ablation process and of the colloid produced after 40 min ablation with 248 nm wavelength, 2.3 Jcm^{-2} laser fluence and 7 Hz RR. The comparison between them showed their perfect match. Future research should shed more light on this issue. The FTIR peak located between 3135-3690 cm^{-1} is assigned for O-H group in choline chloride and ethylene glycol-based DES which is in agreement with the other reported works [48,32]. In the spectrum of the final solution, Pt-NPs and ILEG, the same group (O-H) appears, and it is unchanged. Further, the peaks in the region of 3000-2800 ILEG show the presence of C-H and CH_2 stretching bands. Moreover, a peak at 954 cm^{-1} presents quaternary ammonium group of ChCl and another peak at 1232 cm^{-1} is representing C-N stretching vibration [49]. The presence of Cl^- in DES is shown at 515 cm^{-1} and the FT-IR analysis describes that the establishment of ILEG does not lead to the formation of new functional groups in the mixture which can indicate that the liquid medium used in PLAL is stable and no decomposition/degradation or new substance appear.

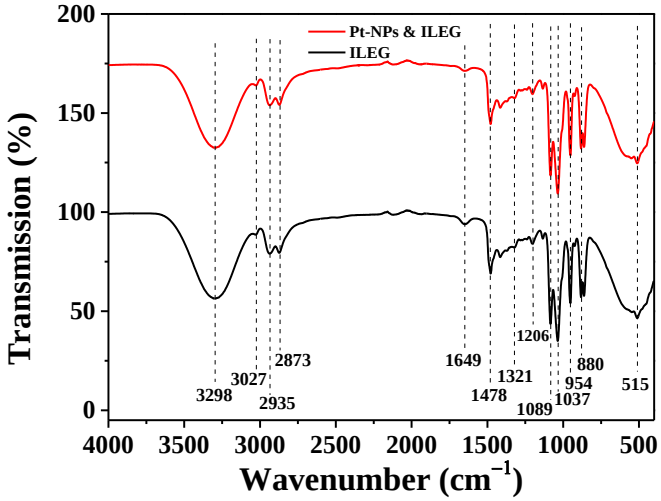

Figure 6.19. FTIR spectra: pure ILEG – black spectrum and fabricated Pt-NPs – red spectrum.

The Raman spectroscopy was performed on the same samples for further analysis and research, as is shown in Figure 6.20. By examining the Raman spectra of ILEG compound, it can be found that the characteristic peaks at 712, 861, 950, 1048, 1085, 1268, 1455, 2881, 2937, 2975 and 3030 cm^{-1} belong to ILEG compound [50]. From the graph, there is no new absorption peak or conspicuous peak shift in the liquid medium after the irradiation with the laser beam. Accordingly, it is preliminarily determined that the laser beam interaction with the solvent does not change inside the organic compound to form new substance. Through FT-IR spectrum and Raman spectrum, the results demonstrate that the PLAL process doesn't transform the composition and molecular structure of the ILEG medium.

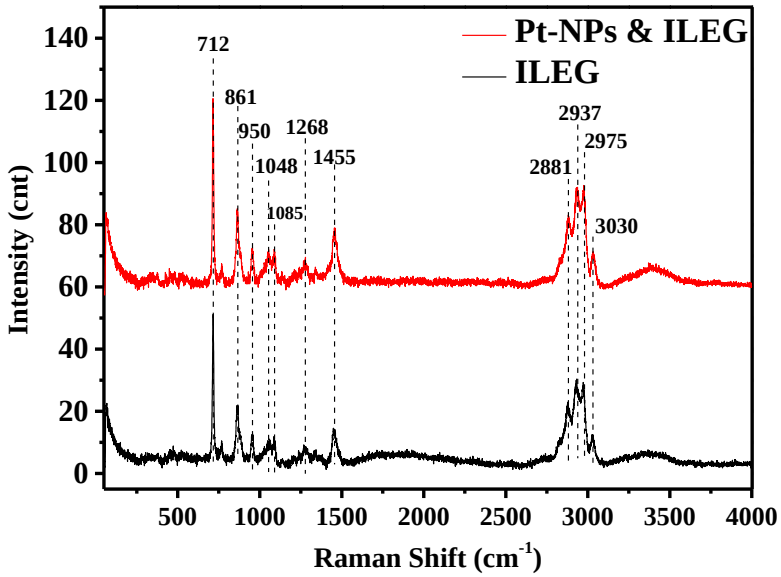

Figure 6.20. Raman spectra: pure ILEG (black curve) and synthesized Pt-NPs (red curve).

6.3.5. Application of the synthesized Pt-NPs

In general, noble metal Pt-NPs have been considered for a long time as inactive substrates for the SERS method, several investigators have reported the use of Pt material as working SERS substrates [35–37]. In this section, the active role of Pt-NPs in the detection of MB was studied. Figure 6.22 shows the Raman spectra of both investigated samples, pure MB (black spectrum) and small Pt-NPs with an average size of 2.2 nm, manufactured with a laser fluence of 2.3 Jcm^{-2}, 7 Hz and for 40 min in pure ILEG (red spectrum), mixed with pure MB and dried on a cover glass. The Raman peaks located near to 466 cm^{-1} and 1625 cm^{-1} were attributed to C-N-C skeletal bending and C-C stretching modes. As can be seen in Figure 21 - black spectrum, the specifics bands of the pigment have very low intensities and are difficult to see. The MB peaks became strong pronounced while involving Pt-NPs, because of the Pt-NPs activity in the pigment.

The proportion between the intensities for MB absorbed in the presence or in the absence of substrate, respectively (I_{SERS}/I_{Ref}) is 11.05 for the main characteristic peak with the highest intensity positioned at 1625 cm^{-1}. The achieved results express a high enhance of the signal of over one order of magnitude.

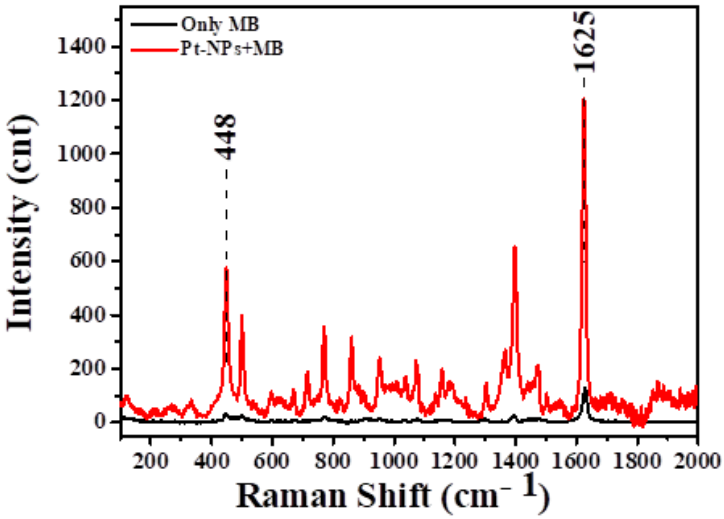

Figure 6.22. Raman spectra of mixed solution between Pt–NPs and MB (red curve) and pure MB (black curve).

CONCLUSIONS

The PhD thesis presents an extensive study of the synthesis of Pt-NPs in different solvents such as double distilled water, aqueous ethanol solution, aqueous isopropanol solution and eutectic solvent based on choline chloride and ethylene glycol (molar ratio 1:2), using the technique of KrF excimer laser ablation and its optimization was successfully achieved for the first time.

Both the impact of laser parameters such as laser fluence, RR, energy transferred to liquid and target, and ablation time on the manufacturing process as well as the optical and morphological characteristics of the fabricated Pt-NPs were investigated.

UV/Vis spectroscopy was performed immediately after each ablation process and the corresponding spectra obtained were discussed in order to determine both the optical properties of and the presence of Pt-NPs in the colloidal solution.

The morphological properties were determined using the HR-STEM technique and the electron images of fully spherical and spherical-like Pt-NPs were reported. The smallest mean diameter values for NPs were determined to be: 2.2 nm in double distilled water, 1.7 nm in

60% ethanol and 80% isopropanol solutions, respectively, and 2.2 nm when the eutectic solvent, ChCl, was used: EG (1:2). These values were obtained when Pt-NPs were synthesized with laser fluence of 2.3 Jcm-2 and RR of 10 Hz, but in the case of ChCl:EG RR of 7 Hz was used.

A linear increase in the diameter of Pt-NPs with respect to the RR used in the synthesis process was established for the first time, at the laser fluence of 2.3 Jcm-2 provided by the KrF excimer laser when bidistilled water was used.

The EDX analysis demonstrated the presence of Pt-NPs along with HR-STEM interplanar distance measurements and complementary XRD. The measured interplanar distances, 0.23, 0.22, 0.19 and 0.12 nm, are specific to the crystal planes (111), (200) and (311) of Pt-NPs with FCC structure. Complementarily, MS-DART was involved to identify the atomic mass of Pt in the colloidal solution.

The synthesis method of Pt-NPs, PLAL, presented in this doctoral thesis is a "top-down" physical method, relatively simple and ecological, which can be easily transferred to the industrial field.

Selective bibliography

Chapter 1

[1] *G. W. Yang*, "Laser ablation in liquids: Applications in the synthesis of nanocrystals", Progress in Materials Science, **vol. 52**, Oct. 2006, pp. 648-698.

[2] *A. Wazeer, A. Das, A. Sinha, A. Karmakar,* "Nanomaterials synthesis via laser ablation in liquid: A review", Journal of the Institution of Engineers, **vol. 104**, Iul. 2022, pp. 413-426.

[3] *T.H. Maiman,* "Stimulated optical radiation in ruby", Nature, **vol. 187**, no. 493, 1960, pp. 134-136.

[4] *L. Zhao, Z. Liu, D. Chen, F. Liu, Z. Yang, X. Li, H. Yu, H. Liu, W. Zhou,* "Laser synthesis and microfabrication of micro/ nanostructured materials toward energy conversion and storage", Nano-Micro Letters, **vol. 13**, no. 49, Ian. 2021, pp. 1-48.

[5] *N. T. K. Thanh, N. Maclean, S. Mahiddine,* "Mechanisms of nucleation and growth of nanoparticles in solution", Chemical Reviews, **vol. 114**, no. 15, Iul. 2014, pp. 7610-7630.

[6] *I. W. Boyd,* "Thin Film Growth by Pulsed Laser Deposition", Laser in der Technik, Springer-Verlag Berlin Heidelberg, 1994, pp. 349-359.

[7] *F. Mafuné, J. Kohno, Y. Takeda, T. Kondow,* "Formation of gold nanonetworks and small gold nanoparticles by irradiation of intense pulsed laser onto gold nanoparticles", Journal of Physical Chemistry B, **vol. 107**, no. 46, Oct. 2003, pp. 12589-12596.

[8] *A. Bratovcic*, "Different applications of nanomaterials and their impact on the environment". SSRG International Journal of Material Science and Engineering (IJMSE), **vol. 5**, no. 1, Apr. 2019, pp. 1–7.

[9] *K. Gajanan, S. N. Tijare*, "Applications of nanomaterials", Materials Today: Proceeding, **vol. 5**, no. 1, 1093–1096.

[10] *L. R. Khot, S. Sankaran, J. M. Maja, R. Ehsani, E. W. Schuster,* "Applications of nanomaterials in agricultural production and Crop Protection: A Review", Crop Protection, **vol. 35**, Mai 2012, pp. 64–70.

[11] *E. Roduner,* "Size matters: Why nanomaterials are different", Chemical Society Reviews, **vol. 35**, no. 7, Mai 2006, pp. 583-592.

[12] *M.G. Lines,* "Nanomaterials for practical functional uses", Journal of Alloys and Compounds, **vol. 449,** no. 1-2, Ian. 2008, pp. 242–245.

[13] *A. Gade, A. Ingle, C. Whiteley, M. Rai*, "Mycogenic metal nanoparticles: Progress and applications", Biotechnology Letters, **vol. 32**, no. 5, Ian. 2010, pp. 593–600.

[14] *C. Buzea, I. I. Pacheco, K. Robbie,* "Nanomaterials and nanoparticles: Sources and toxicity", Biointerphases, **vol. 2**, no. 4, Dec. 2007, MR17-MR71.

[15] *M.A. Ashraf, W. Peng, Y. Zare, K. Y. Rhee,* "Effects of size and aggregation/agglomeration of nanoparticles on the interfacial/interphase properties and tensile strength of polymer nanocomposites", Nanoscale Research Letters, **vol. 13**, no. 214, Iul. 2018, pp. 1-7.

Chapter 3

[1] *S. Moniri, M. R. Hantehzadeh, M. Ghoranneviss, M. A. Asadabad*, "Study of the optical and structural properties of Pt nanoparticles prepared by laser ablation as a function of the applied electric field", Applied Physics, **vol. 123,** no. 684, 2017, pp. 1-11.

[2] *M. I. Mendivil Palma, B. Krishnan, G. A. C. Rodriguez, T. K. Das Roy, D. A. Avellaneda, S. Shaji,* "Synthesis and Properties of Platinum Nanoparticles by Pulsed Laser Ablation in Liquid", Journal of Nanomaterials, **vol. 2016**, 2016, pp. 1-11.

[3] *N. Thondavada, R. Chokkareddy, G. G. Redhi*, "Green synthesis of platinum nanoparticles and their biomedical applications", Green Metal Nanoparticles, 2018, pp. 603-627.

[4] *B. Lu, Q. Liu, F. Nichols, R. Mercado, D. Morris, N. Li, P. Zhang, P. Gao, Y. Ping, S. Chen,* "Oxygen Reduction Reaction Catalyzed by Carbon-Supported Platinum Few-Atom Clusters: Significant Enhancement by Doping of Atomic Cobalt", Research, **vol. 2020**, 2020, pp. 1-12.

[5] *M.Stratmann, J.Müller*, "The mechanism of the oxygen reduction on rust-covered metal substrates", Corrosion Science, **vol. 36**, 1994, pp. 327-359.

[6] *T. Zhang, Y. Hu, Y. Zhou, X. Gong, Z. Wang, S. Zhang, M. Wang*, "Oxygen Reduction Reaction from Water Electrolysis Intensified by Pressure and O_2− Oxidation Desulfurization", Journal of The Electrochemical Society, **vol. 165**, no. 5, 2018, pp. 139-147.

[7] *M. Liu, L. Wang, K. Zhao, S. Shi, Q. Shao, L. Zhang, X. Sun, Y. Zhao, J. Zhang*,"Atomically dispersed metal catalysts for the oxygen reaction: synthesis, characterization, reaction mechanisms and electrochemical energy applications", Energy & Environmental Science, **vol. 12**, 2019, pp. 2890-2923.

[8] *J. N. Tiwari, K. Nath,S. Kumar, R. N. Tiwari, K. C. Kemp, N. H. Le, D. H. Youn, J. Sung Lee, K. S. Kim*, "Stable platinum nanoclusters on genomic DNA-graphene oxide with a high oxygen reduction reaction activity", Nature Communications, **vol. 4**, no. 2221, 2013, pp. 1-7.

[65] *M. Hiramatsu, M. Hori*, "Preparation of dispersed platinum nanoparticles on a carbon nanostructured surface using supercritical fluid chemical deposition", Materials, **vol. 3**, 2010, pp. 1559-1572.

[66] *Y. W. Ma, Z. R. Liu, B. L. Wang, L. Zhu, J. P. Yang, X. A. Li*, "Preparation of graphene-supported Pt-Co nanoparticles and their use in oxygen reduction reactions", Xinxing Tan Cailiao/New Carbon Mater., **vol. 51**, 2013, pp. 435-438.

[67] *S. Liang, Y. Xia, S. Zhu, S. Zheng, Y. He, J. Bi, M. Liu, L. Wu,* "Au and Pt co-loaded g-C 3 N 4 nanosheets for enhanced photocatalytic hydrogen production under visible light irradiation", Appl. Surf. Sci., **vol. 358**, 2015, pp. 304-312.

[68] *Y. Fan, P. F. Liu, Z. J. Yang, T. W. Jiang, K. L. Yao, R. Han, X. X. Huo, Y. Y. Xiong*, "Bi-functional porous carbon spheres derived from pectin as electrode material for supercapacitors and support material for Pt nanowires towards electrocatalytic methanol and ethanol oxidation", Electrochim. Acta., **vol. 163**, 2015, pp. 140-148.

[69] *W. Huang, H. Wang, J. Zhou, J. Wang, P. N. Duchesne, D. Muir, P. Zhang, N. Han, F. Zhao, M. Zeng, J. Zhong, C. Jin, Y. Li, S.T. Lee, H. Dai*, "Highly active and durable methanol oxidation electrocatalyst based on the synergy of platinum-nickel hydroxide-graphene", Nat. Commun., **vol. 6**, no. 10035, 2015, pp. 1-8.

Chapter 4

[12] *A. Tąta, B. Gralec, E. Proniewicz*, "Unsupported platinum nanoparticles as effective sensors of neurotransmitters and possible drug curriers", Applied Surface Science, **vol. 435**, 2018, pp. 256-264.

[13] *R. Gómez, J. Solla-Gullón, J.M. Pérez, A. Aldaz*, "Nanoparticles-on-electrode approach for in situ surface-enhanced Raman spectroscopy studies with platinum-group metals: Examples and prospects", Journal of Raman Spectroscopy, **vol. 36**, 2005, pp. 613-622.

[46] *J. Bandak, J. Petzold, H. Hatahet, A. Prager, B. Kersting, C. Elsner, B. Abel*, "Interconnected electrocatalytic Pt-metal networks by plasma treatment of nanoparticle-peptide fibril assemblies", RSC Adv., **vol. 9**, 2019, pp. 5558–5569.

[47] *W. Ji, W. Qi, S. Tang, H. Peng, S. Li*, "Hydrothermal synthesis of ultrasmall Pt nanoparticles as highly active electrocatalysts for methanol oxidation", Nanomaterials, **vol. 5**, 2015, pp. 2203-2211.

[48] *M. Naresh Kumar*, "Green Synthesis and Characterization of Platinum Nanoparticles using Sapindus mukorossi Gaertn. Fruit Pericarp", Asian Journal of Chemistry, **vol. 29,** 2017, pp. 2541-2544.

[49] *M. Naresh Kumar*, " Green synthesis and characterization of platinum nanoparticles using sapindus mukorossi Gaertn. Fruit Pericarp" Asian J. Chem. **vol. 29**, 2017, pp. 2541-2544.

Chapter 5

[31] *A. Tąta, B. Gralec, E. Proniewicz*, „Unsupported platinum nanoparticles as effective sensors of neurotransmitters and possible drug curriers", Appl. Surf. Sci., **vol. 435**, 2018, pp. 256-264. https://doi.org/10.1016/j.apsusc.2017.11.100.

[32] *Z.Q. Tian, Z.L. Yang, B. Ren, J.F. Li, Y. Zhang, X.F. Lin, J.W. Hu, D.Y. Wu,* „Surface-enhanced Raman scattering from transition metals with special surface morphology and nanoparticle shape", in: Faraday Discuss, **vol. 132**, 2006, pp. 159-170. https://doi.org/10.1039/b507773g.

[33] *R. Gómez, J. Solla-Gullón, J.M. Pérez, A. Aldaz,* „Nanoparticles-on-electrode approach for in situ surface-enhanced Raman spectroscopy studies with platinum-group metals: Examples and prospects", J. Raman Spectrosc., **vol. 36**, 2005, pp. 613-622. https://doi.org/10.1002/jrs.1377.

Chapter 6

[35] *R. Gómez, J. Solla-Gullón, J.M. Pérez, A. Aldaz*, Nanoparticles-on-electrode approach for in situ surface-enhanced Raman spectroscopy studies with platinum-group metals: Examples and prospects, J. Raman Spectrosc.. **vol. 36**, 2005, pp. 613-622. https://doi.org/10.1002/jrs.1377.

[36] *E. Kämmer, T. Dörfer, A. Csáki, W. Schumacher, P.A. da Costa Filho, N. Tarcea, W. Fritzsche, P. Rösch, M. Schmitt, J. Popp*, Evaluation of colloids and activation agents for determination of melamine using UV-SERS, J. Phys. Chem. C., **vol. 116**, 2012, pp. 6083–6091. https://doi.org/10.1021/jp211863y.

[37] *L. Deng, M.T. Nguyen, T. Yonezawa*, „Sub-2 nm Single-Crystal Pt Nanoparticles via Sputtering onto a Liquid Polymer", Langmuir, vol. 34, 2018, pp. 2876–2881. https://doi.org/10.1021/acs.langmuir.7b04274.

[43] *N. Peeters, K. Janssens, D. de Vos, K. Binnemans, S. Riaño,* „Choline chloride–ethylene glycol based deep-eutectic solvents as lixiviants for cobalt recovery from lithium-ion battery cathode materials: Are these solvents really green in high-temperature processes?", Green Chem., **vol.24(17)**, 2022, pp. 6685–6695. doi:10.1039/d2gc02075k.

[44] *S.L. Perkins, P. Painter, C.M. Colina*, „Molecular dynamic simulations and vibrational analysis of an Ionic liquid analogue", J. Phys. Chem. B, **vol. 117(35),** 2013, pp. 10250–10260. doi:10.1021/jp404619x.

[45] *M. Saha, M.S. Rahman, M.N. Hossain, D.E. Raynie, M.A. Halim*, „Molecular and spectroscopic insights of a choline chloride based therapeutic deep eutectic solvent", J. Phys. Chem. A, **vol.124(23)**, 2020, pp. 4690–4699. doi:10.1021/acs.jpca.0c00851.

[46] *C. Rong, X. Juncai, W. Xinyang, M. Qiang, S. Huaneng, Y. Weiwei, X. Qian*, „Electrochemical Characteristics and Transport Properties of V(II)/V(III) Redox Couple in a Deep Eutectic Solvent: Magnetic Field Effect", Front. Chem., **vol. 8,** 2020, articol **619.** doi.org/10.3389/fchem.2020.00619

IF, AIS AND SRI CENTRALIZER TABLE OF PUBLISHED WORKS

1. G. Li, A. Iakunkov, N. Boulanger, **O.A. Lazăr**, M. Enăchescu, A. Grimm, A. V. Talyzin, "Activated carbons with extremely high surface area produced from cones, bark and wood using the same procedure", RSC Advances, Vol. 13(21), pp. 14543-14553, 2023.

2. **O. A. Lazăr**, A. S. Nikolov, C. C. Moise, G. V. Mihai, M. Prodana, M. Enăchescu, "KrF excimer laser for Pt–NPs synthesis by PLAL in isopropanol solution and their use in a SERS application", Journal of Materials Research and Technology, Vol. 24(4), pp. 7135-7152, 2023.

3. **O. A. Lazăr,** A. S. Nikolov, C. C. Moise, S. Rosoiu, M. Prodana, M. Enăchescu, "Fabrication of Pt nanoparticles by nanosecond pulsed laser ablation in aqueous solution of ethanol using KrF excimer laser", Applied Surface Science, Vol. 609, 155289, 2023.

4. **O. A. Lazăr**, C. C. Moise, A. S. Nikolov, L. B. Enache, G. V. Mihai, M. Enachescu, "The Water-Based Synthesis of Platinum Nanoparticles Using KrF Excimer Laser Ablation", Nanomaterials, Vol. 12(3), 348, 2022.

5. A. T.S.C. Brandão, S. Rosoiu, R. Costa, **O. A. Lazăr**, A. F. Silva, L. Anicai, C. M. Pereira, M. Enăchescu, "Characterization and electrochemical studies of MWCNTs decorated with Ag nanoparticles through pulse reversed current electrodeposition using a deep eutectic solvent for energy storage applications", Journal of Materials Research and Technology, Vol. 15, pp. 342-359, 2021.

6. C. C. Moise, L. B. Enache, V. Anăstăsoaie, **O. A. Lazăr**, G. V. Mihai, M. Bercu, M. Enăchescu, "On the growth of copper oxide nanowires by thermal oxidation near the threshold temperature at atmospheric pressure", Journal of Alloys and Compounds, Vol. 886, pp. 161130, 2021.

7. C. C. Moise, L. Rachmani, G. Mihai, **O. Lazăr**, M. Enăchescu, N. Naveh, "Pulsed Laser Deposition of SWCNTs on Carbon Fibres: Effect of Deposition Temperature", Polymers, Vol. 13(7), pp.1138, 2021.

8. A. Barra, **O. Lazăr**, A. Pantazi, M. J. Hortigüela, G. Otero-Irurueta, M. Enăchescu, E. Ruiz-Hitzky, C. Nunes, P. Ferreira, "Joining Caffeic Acid and Hydrothermal Treatment to Produce Environmentally Benign Highly Reduced Graphene Oxide", Nanomaterials, vol. 11(3), pp. 732, 2021.

9. A. Cernat, A. Petica, V. Anastasoaie, **O. Lazăr**, S. J. Györfi, M. B. Irimes, G. Stefan, M. Tertis, Marius Enachescu b, Liana Anicăi b, Cecilia Cristea a, "Detection of hydrogen peroxide involving bismuth nanowires via template-free electrochemical

synthesis using deep eutectic solvent", Electrochemistry Communications, Vol. 121, pp. 106869, 2020.

10. **O. A. Lazăr**, A. Marinoiu, M. Raceanu, A. Pantazi, G. Mihai, M. Varlam, M. Enachescu, "Reduced Graphene Oxide Decorated with Dispersed Gold Nanoparticles: Preparation, Characterization and Electrochemical Evaluation for Oxygen Reduction Reaction", Energies, Vol. 13(17), pp. 4307, 2020.

11. G. Melinte, A.Cernat, A. Petica, **O. Lazăr**, M. Enachescu, L. Anicai, C. Cristea, "Electrochemical Non-Enzymatic Detection of Glucose Based on 3D Electroformed Copper on Ni Foam Nanostructures", Materials, Vol. 13(12), pp. 2752, 2020.

12. A. Stanke, V. Kampars, **O.A. Lazăr**, M. Enachescu, "Preparation and Characterization of Fe2O3/ SBA-15 for Fischer-Tropsch Process", Key Engineering Materials, Vol 850, pp.144-150, 2020.

13. A. T. S. C. Brandão, L. Anicai, **O. A. Lazăr**, S. Rosoiu, A. Pantazi, R. Costa, M. Enachescu, C. M. Pereira, A. F. Silva, "Electrodeposition of Sn and Sn Composites with Carbon Materials Using Choline Chloride-Based Ionic Liquids", Coatings, Vol. 9(12), pp. 798, 2019.

14. A. Barra, N. M. Ferreira, M. A. Martins, **O. Lazăr**, A. Pantazi, A. A. Jderu, S. M. Neumayer, B. J. Rodriguez, M. Enăchescu, P. Ferreira, C. Nunes, "Eco-friendly preparation of electrically conductive chitosan - reduced graphene oxide flexible bionanocomposites for food packaging and biological applications", Composites Science and Technology, Vol. 173, pp. 53-60, 2019.

15. S. Inaba, R. Arai, G. Mihai, **O. Lazăr**, C. Moise, M. Enachescu, Y. Takeoka, V. Vohra, "Eco-Friendly Push-Coated Polymer Solar Cells with No Active Material Wastes Yield Power Conversion Efficiencies over 5.5", ACS Appl Mater Interfaces, Vol. 20(11), pp. 10785-10793, 2019.

16. M. Iovu, V. Verlan, O. Bordian, M. Enăchescu, A. Popescu, D. Savastru, L. B. Enache, S. Roșoiu, M. Bardeanu, **O. A. Lazăr**, G. Mihai, "Synthesis of glassy composite As0.63S2.70Sb1.37Te0.30 and its physical properties", Optoelectronics and Advanced Materials, Rapid Communications, 2022, nr. 11-12(16), pp. 538-544. ISSN 1842-6573.

17. O. V. Iaseniuc, M. S. Iovu, A. Pantazi, **O. A. Lazăr**, C. C. Moise, M. Enăchescu," Assessing the structural properties of GexAsxSe1-2x chalcogenide systems through cross-correlated STEM, XRD and micro-Raman studies", Optoelectronics and Advanced Materials - Rapid Communications, 15, 9-10, September-October 2021, pp.498-503 (2021).

18. M. Iovu, I. Culeac, V. Verlan, Olga Bordian, M. Enachescu, A. A. Popescu, D. Savastru, **A. Lazăr**, "Synthesis and optical properties of the glassy compound As0.63S2.70Sb1.37Te0.30 ", Chalcogenide Letters Vol. 20, No. 5, p. 387 - 392 (2023).

Capitole de Cărți

19. **O. A. Lazăr,** A. S. Nikolov, C. C. Moise, M Enăchescu,"Pulsed Laser Ablation in Liquids for fabrication of noble metal nanostructures", în Laser Ablation, IntechOpen, United Kingdom, 2023 (under publication, http://dx.doi.org/10.5772/intechopen.111550).
20. A. Marinoiu, G. Mihai, **O. A. Lazăr**, S. Roșoiu, M. Prodana, C. Sisu, M. Răceanu, M. Enăchescu, "Facile preparation of graphene-supported platinum-cobalt nanoparticles and their use as electrocatalyst in PEM fuell cells" în Nanomaterials – functional properties and applications, ed. Academiei Române, București, 2020, vol. 9-38.

LIST OF PRESENTATIONS AT INTERNATIONAL CONFERENCES

1. L. B. Enache, G. Mihai, **O. Lazăr,** S. Rosoiu, A. G. Pantazi, C. Moise, A. A. Messina, M. Enachescu, Stress analysis by XRD and Raman on different semiconductor substrates, 9th International Congress on Microscopy & Spectroscopy (INTERM), 21-29 apr 2022, (P), Oludeniz, Turcia.

2. A. Barra, C. Ruiz-García, C. Bratu, **O. Lazăr**, G. Mihai, M. Darder, P. Aranda, M. Enăchescu, C. Nunes, P. Ferreira, E. Ruiz-Hitzky, "Eco-friendly synthesis of a porous graphene-like material supported on clay", NanoSpain2023, (P), April 25-28, 2023, Tarragona (Spain)

3. G. Mihai, C. Moise, O**. Lazăr,** V. Anastasoaie, L. B. Enache, S. Rosoiu, M. Vardaki, A. Pantazi, M. Enachescu, *GaN NANOSTRUCTURING*, The 5th International Conference New Trends on Sensing - Monitoring - Telediagnosis for Life Sciences NT-SMT-LS 2020, 3-4 Iulie NOMARES, București, România, ONLINE, (OP) O.4.3.

4. **O. Lazăr,** C. Moise, G. Mihai, L. B. Enache, A. Pantazi, M. Enachescu, *Heavy Metals Ions Detection on Azulene-Azothiadiazole Based CMEs*, The 5th International Conference New Trends on Sensing - Monitoring - Telediagnosis for Life Sciences NT-SMT-LS NOMARES, 3-4 Iulie 2020, București, România, ONLINE, (OP) O.4.6. – **premiul I pentru cea mai bună prezentare orală**.

5. L. B. Enache, C. Moise, V. Anastasoie, G.Mihai, **O. Lazăr**, E. M. Ungureanu, L. Anicai, M. Enachescu, *Platinum Nanoparticles as Smart Catalyst Synthesized by Krf Laser Ablation in Liquids*, 9th International Conference of the Chemical Societies of the South-East European Countries, (P), May 8th – 11th, 2019, Târgoviște.

6. A. Petica, V. Anastasoaie, **O. Lazăr**, M. Enăchescu, T. Visan, L. Anicai, Electrochemical synthesis of 1D bismuth nanostructures using deep eutectic solvents, 21st Romanian International Conference on Chemistry and Chemical Engineering, (P), 4 – 7 Septembrie, 2019, Constanța.

7. M. Prodana, D. Ionita, C. Moise, **O. Lazăr**, M. Enăchescu, Carbon nano-onions in biomedical applications, 21st Romanian International Conference on Chemistry and Chemical Engineering, (P), 4 – 7 Septembrie, 2019, Constanța.

8. A. Cojocaru, S. P. Rosoiu, **O. Lazăr**, G. Mihai, A. Pantazi, M. Enachescu, L. Anicai, T. Visan, Electrodeposition of nickel-cobalt Aalloy / MWCNT composite coatings involving deep eutectic solvents, 21st Romanian International Conference on Chemistry and Chemical Engineering, (P), 4 – 7 Septembrie, 2019, Constanța.

9. G. Mihai, C. Moise, A. Pantazi, **O. Lazăr**, Ș. Marin and M. Enăchescu "Manufacturing and dispersion of SWCNTs as a prerequisite for nanodevice building using Electron Beam Lithography", Bucharest CA 15107 Fall Meeting on Multi-Functional Nano-Carbon Composite Materials, 6-7 Septembrie 2018, University Politehnica of Bucharest, Bucuresti, Romania. (P);

10. A. Marinoiu, **O. A. Lazăr**, A. Pantazi, G. Mihai and M. Enachescu "Platinum decorated reduced graphene oxide for PEM fuel cells applications",Bucharest CA 15107 Fall Meeting on Multi-Functional Nano-Carbon Composite Materials, 6-7 Septembrie 2018, University Politehnica of Bucharest, Bucuresti, Romania. (P);

11. G. Mihai, C. Moise, A. Pantazi, A. Jderu, O. Tutunaru, R. Mesterca, **O. Lazăr**, A. Pumnea, D. Dorobantu and M. Enachescu "Optimization of PMMA Processing as a

prerequisite for nanodevice building using Electron Beam Lithography", International Conference CHIMIA 2018 "New Trends in Applied Chemistry" - Ovidius University of Constanta , 24-26 Mai 2018,Constanta, Romania. (OP);

12. A. Pantazi, A. Jderu, R. Mesterca, G. Mihai, **O. Lazar**, S. Marin, O. Tutunaru, D. Dorobantu, A. Pumnea and M. Enachescu "Adhesive properties studies of f-SWCNTs based nanocomposite thin films", International Conference CHIMIA 2018 "New Trends in Applied Chemistry" - Ovidius University of Constanta, 24-26 Mai 2018, Constanta, Romania. (OP);